A Measurement of The Isolated Direct Photon Cross Section at 630 GeV

Michael Strauss
University of Oklahoma, Norman, OK
Sebastian Grinstein, Ricardo Piegaia
Universidad de Bs.As., Argentina

DØ NOTE # 3699
December 10, 1999
Preliminary Version 1.3

Abstract

The inclusive cross section for isolated photons at $\sqrt{s} = 630$ GeV (Run 1c) is measured for the central ($|\eta| < 0.9$) and forward ($1.6 < |\eta| < 2.5$) rapidity regions. We compare the result with next to leading order QCD predictions using CTEQ4 parton distibution functions.

1 Introduction

The present analysis has been developed along the lines of the published Run 1A data [1], described in greater detail in a DØ note by S. Linn [2] with variations and improvements incorporated into the Run 1B analysis described in the thesis by S. Jerger [3], as well as other subsequent improvements [4]. In addition, some of the analysis and techniques are reproduced from an earlier DØ note [5] and a Master's thesis written by one of the authors [6]. However, this note supercedes and expands on those previous analyses. The differential cross section for the process $p\overline{p} \rightarrow \gamma + X$ can be written as

$$\frac{d^2\sigma}{dE_T d\eta} = \frac{N\mathcal{P}}{L\Delta\eta\Delta E_T A\epsilon_s\epsilon_d\epsilon_t} \quad (1)$$

where N is the number of photon candidates (one or two per event), $\mathcal{P}$ is the photon purity (the fraction of direct photons in the sample), L is the integrated luminosity, $\Delta\eta$ and ΔE_T are the bin sizes in pseudorapidity and E_T , A is the geometric acceptance, ϵ_s is the efficiency of the selection cuts, ϵ_d is the efficiency of the charged track cut, and ϵ_t is the efficiency of the trigger.

Previous measurments of the isolated single photon cross section at collider energies by UA2 and CDF showed a discrepency between the theory and the data, particularly in the low E_T regions as shown in Fig. 1 [7][8]. The CDF data has never been published.

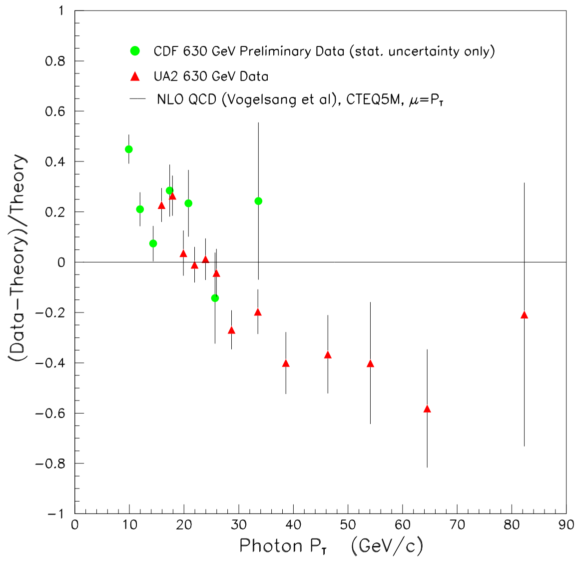

Figure 1: Production of direct photons at 630 GeV from UA2 and CDF. The data is normalized to CTEQ5 as implemented by Vogelsang.

2 Data and Monte Carlo Sample

2.1 The Direct Photon Data Set

The data in this analysis were taken at 630 GeV during the last part of Run 1C, with three dedicated isolated photon triggers, as summarized on Table 1. The respective luminosities, number of events successfully reconstructed, and events used in the analysis after cuts, is also shown.

L1 Trigger	L2 Filter	Thresh. (GeV)	$\int L\,dt$ (nb^{-1})	Events	Events Used
em_1_2_lnr	gam_4_iso5	4.5	2.021	52771	1890
em_1_3_lnr	gam_8_iso3	8	17.22	20597	1169
em_1_7_lnr	gam_14_iso	14	520.5	24362	3161

Table 1: 630 GeV isolated photon triggers

2.2 Monte Carlo Sample

The analysis depends heavily on the Monte Carlo to determine efficiencies and the background from neutral mesons. The MC sample, generated in the Florida State University farm, consists of full PYTHIA photon and electromagnetic jet events, with zero bias events superimposed. To minimize computing time, most of these events only had the particles and energy in a cone of $R = 0.7$ around each photon or jet simulated through DØGEANT, using plate level calorimeter geometry. These events were used to estimate the photon purity, $\mathcal{P}$ (see Section 4). A smaller number of events had the entire event simulated in the detector and are used for determining selection efficiencies, (see Section 3.4).

In an attempt to maximize MC statistics within the allotted cpu budget, about ten different minimum bias events were overlayed for the same PYTHIA event. Although the events in this MC sample are clearly not independent, studies have indicated only a moderate degree of correlation [9]. We will address this point later in greater detail. The number of available MC events is summarized in Tables 2 and 3 for six E_T ranges, in the central and forward regions, respectively

The ability of the MC to model the data was tested by comparing 40 GeV simulated electrons with electron candidates from $W \rightarrow e\nu$ Run 1B events [3]. As there are very few W events for the 630 GeV sample, this comparison could not be performed with the runs corresponding to the data used for the present analysis. However, a comparison of the effect of selections on data and Monte Carlo demonstrated that within statistical accuracy, the two samples were affected in a similar manner.

2.3 Event Selection

The selections used on the MC sample (where applicable) and data are:

E_T **Range**	*Before All Cuts*			*After All Cuts*		
	Data	**MC** γ	**MC Jets**	**Data**	**MC** γ	**MC Jets**
6 – 8	6681	12746	32061	908	6262	7144
8 – 13	8817	26199	42169	742	14862	9495
13 – 18	5719	15731	22566	967	10015	6038
18 – 23	3091	17694	15017	865	12188	4559
23 – 33	1516	19423	15977	377	13074	4908
>33	432	41442	24578	67	29542	8078

Table 2: Number of Data and MC events in central rapidity region as a fundtion of E_T , used for calculatinf photon purity.

E_T **Range**	*Before All Cuts*			*After All Cuts*		
	Data	**MC** γ	**MC Jets**	**Data**	**MC** γ	**MC Jets**
6 – 8	4614	2590	14081	599	1625	3674
8 – 11	5734	13903	17244	313	9188	3880
11 – 15	3036	16830	15914	238	11255	3590
15 – 20	5246	16293	18104	821	11239	4187
20 – 26	1361	17873	12162	256	12501	3129
>26	334	36490	27848	67	25544	7389

Table 3: Number of Data and MC events in forward rapidity region as a function of E_T , bin used for calculating photon purity.

- $|\eta| < 0.9$ ($1.6 < |\eta| < 2.5$) for the central (forward) region.
- $|\eta^{det}| < 9$ ($16 < |\eta^{det}| < 25$) for the central (forward) region.
- $|Z_{vertex}| < 50\,cm$
- For the central region, $0.1 < \mathrm{mod}(16\phi/\pi) < 0.9$.
- No charged track in the CDC.
- $\frac{EM\,E^{R\leq 0.2}}{Total\,E^{R\leq 0.2}} < 0.96$
- Isolation cut: $E_T^{R\leq 0.4} - E_T^{R\leq 0.2} < 2.0\,GeV$.
- H-matrix $\chi^2 < 150$

The first four cuts are labeled acceptance cuts because they constrain the candidate photon and its surrounding cone of isolation to the geometric regions where the detector is well understood. The last three, collectively named selection cuts, are tuned to selectively reject QCD jet contamination in the candidate sample.

3 Calculation of efficiencies

3.1 Trigger Efficiency

The trigger efficiency for the high and medium energy triggers has been determined from the data, while the low-energy trigger efficiency has been determined using Monte Carlo events. The inability to determine the low-energy trigger efficiency with data is one of the weaknesses of this analysis. The sensitivity of the cross section to this correction from Run 1A is shown in Fig. 2. Unfortunately, the isolation requirements in the trigger were different for Run 1A and Run 1C, and to minimize the effect of the uncertainty in the low-energy triggers, we have chosen not to use all the low threshhold data in the final cross section.

This analysis relies on a common method to determine the high energy (14 GeV) and medium energy (8.0 GeV) trigger efficiencies, and on a complementary method to check the high energy trigger efficiency. The results from the two methods are averaged together and their difference is taken as a measure of the systematic uncertainty.

The common method used by the medium and high energy triggers simply takes the ratio of the number of 14 GeV (8.0 GeV) triggers divided by the

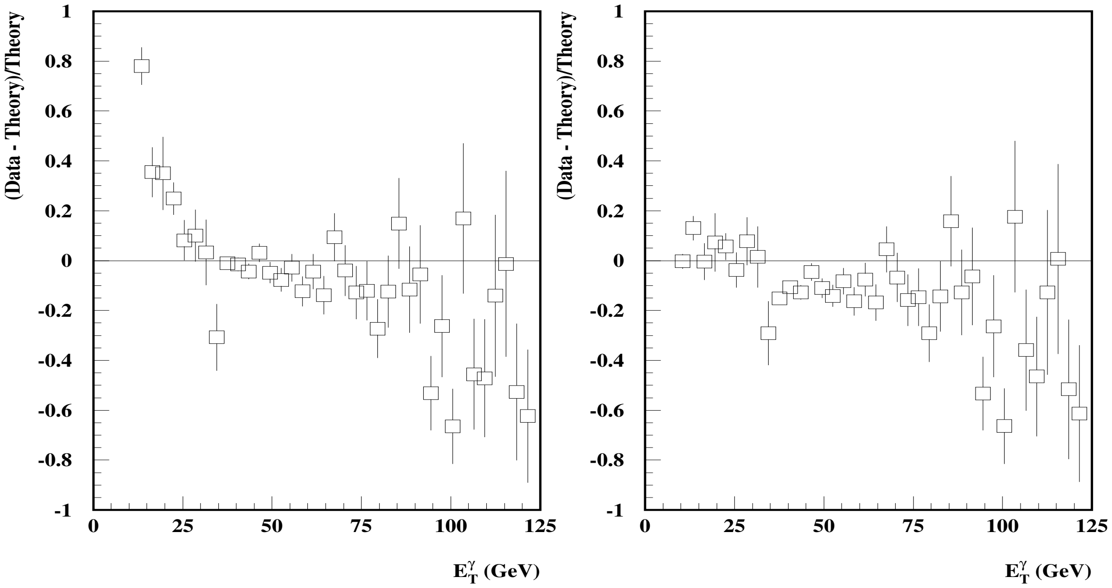

Figure 2: Effect of trigger efficiency on Run 1A data. *Left*: Published result for the CC region. *Right*: Same data, but without the correction for trigger efficiency.

number of 8.0 GeV (4.5 GeV) triggers, with both triggers multiplied by the appropriate pre-scale factors taken from the run. The trigger turn on ratios are shown in Fig. 3 and Fig. 4 for the CC and EC, respectively.

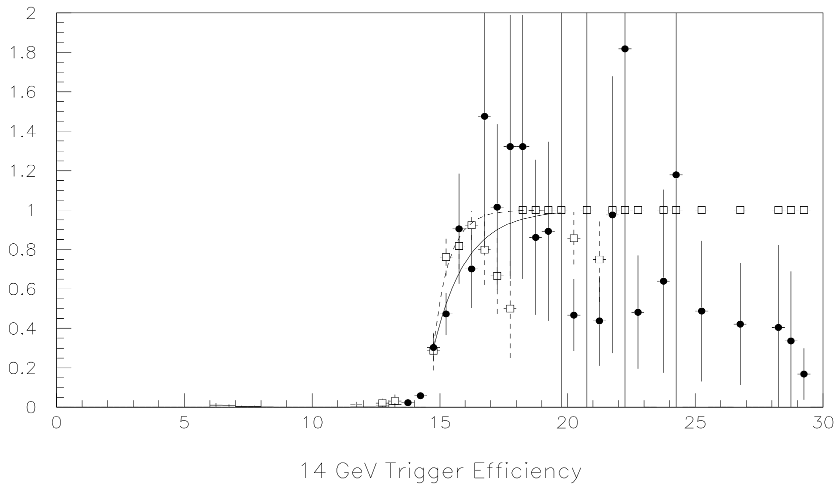

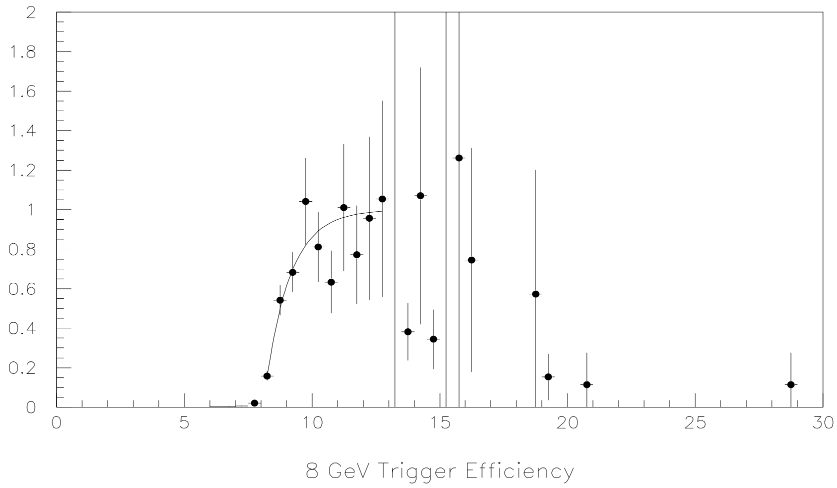

Figure 3: Trigger efficiency for the central region. The black circles show the efficiency determined from the prescale-corrected data described in the text, and the open squares show the efficiency determined from the direct method that is only applicable to the high energy trigger.

The alternative method for finding the high energy efficiency uses all events that fired the medium energy trigger. The fraction of medium energy triggered events that also fired the high trigger defines the efficiency. This can only be used for the high energy trigger because it was not prescaled. This alternative method is also shown in Fig. 3 and Fig. 4.

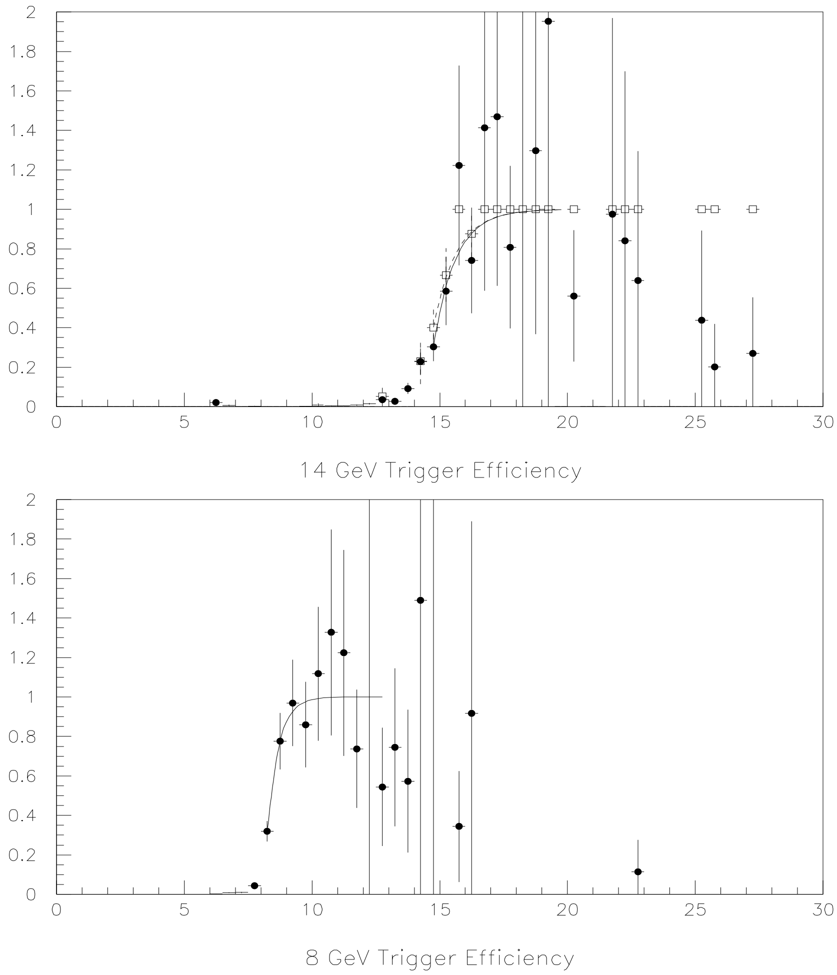

Figure 4: Trigger efficiency for the forward region. The black circles show the efficiency determined from the prescale-corrected data described in the text, and the open squares show the efficiency determined from the direct method only applicable to the high energy trigger.

The points were fitted with a functional form

$$\epsilon_t = 1 - e^{(b-E_T)/a} \tag{2}$$

where a and b are free parameters, with b approximately equal to the trigger threshold energy.

Note that for the EC, the two methods of determining the high energy trigger efficiency give almost identical results, while for the CC, the fit results differ by 1.3σ. As mentioned earlier, the quoted result for the high energy trigger is the average of the two methods. The systematic uncertainty is defined by the difference between the method.

It is not possible to determine the low energy efficiency from the data, so instead we have used results of a MC study carried on by A. Schaffer in 1995 [10], with events generated for the Run 1A analysis, both for the central and forward rapidity regions.

The low energy trigger efficiency is shown in Fig. 5. The points have been fitted with the functional form in Eq. 2 with $a = 1.97 \pm 0.32$ (1.80 ± 0.30) in the central (forward) region and b set to the threshold energy of 4.5 GeV. The error bands have been enlarged to account for other possible functional dependences. The trigger efficiencies used in this analysis are summarized in Table 4. The uncertainty in the determination of the trigger efficiency below 10 GeV is just one of the very large systematic errors that effect the low-E_T region. In addition, there is a large background fraction and the determination of the purity in the low-E_T data is imprecise, (Section 4). Also, the selection efficiency is not well determined below 8 GeV (section 3.4). Because of these three problems, we have chosen 8 GeV as the minimum E_T for quoting a cross section.

Threshold	**Region**	**a**	**b**
4.5 GeV	CC	1.97 ± 0.32	4.5
8.0 GeV	CC	$1.01 \pm 0.19 \pm 0.08$	$8.07 \pm 0.05 \pm 0.04$
14.9 GeV	CC	$0.96 \pm 0.34 \pm 0.32$	$14.41 \pm 0.22 \pm 0.20$
4.5 GeV	EC	1.80 ± 0.32	4.5
8.0 GeV	EC	$0.45 \pm 0.16 \pm 0.32$	$8.08 \pm 0.07 \pm 0.04$
14.9 GeV	EC	$0.88 \pm 0.17 \pm 0.05$	$14.36 \pm 0.18 \pm 0.19$

Table 4: Trigger efficiency used for this analysis. Fit to the functional form $\epsilon_t = 1 - e^{(E_T-b)/a}$. The first error is statistical and the second is systematic.

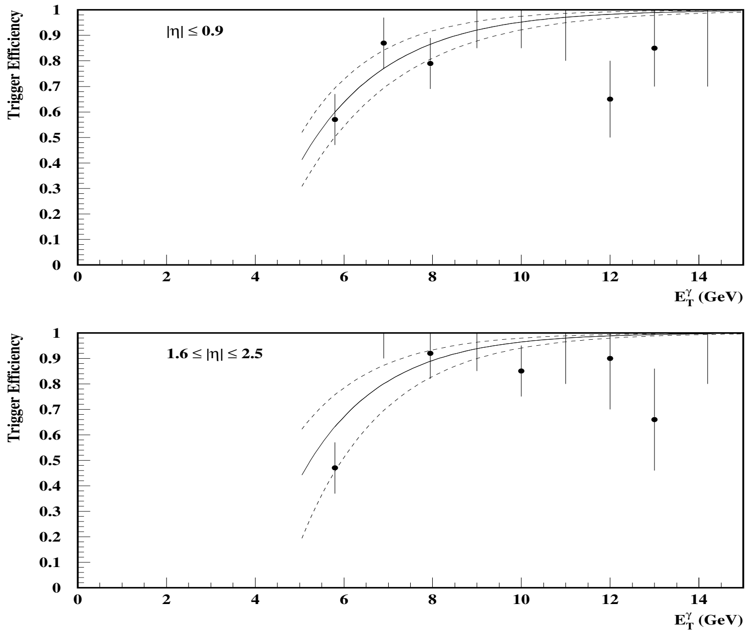

Figure 5: Low energy trigger efficiencies for the central and forward regions.

3.2 Acceptance cuts

The acceptance A takes into account the events lost due to the cuts in the cracks of ϕ module (20% in the CC), in the Z_{vertex} distribution, and in η.

The acceptance in Z_{vertex} was estimated both by taking the ratio of events with and without the selection, and by fitting the vertex distribution shown in Fig. 6 to a Gaussian function. The resulting efficiency is defined by the average of the two methods, 0.854 ± 0.006 ($.848 \pm .004$) for the CC (EC), with a systematic error defined by the difference between the two.

The acceptance in η_d was taken from the Run 1B analysis, and is 0.917 ± 0.007 (0.930 ± 0.007) in the central (forward) region [3]. It was calculated from a MC simulation, using an η distribution modeled by Owens et al. [11]. The systematic uncertainty corresponds to the difference obtained for a flat distribution in physics η and the above distribution. This systematic uncertainty is large enough to encompass any minor differences in shape between the 1800 and 630 GeV distributions.

Combining the three separate sources of loss, the total acceptance is $A = 0.626 \pm 0.007$ (0.789 ± 0.007) in the central (forward) pseudorapidity region.

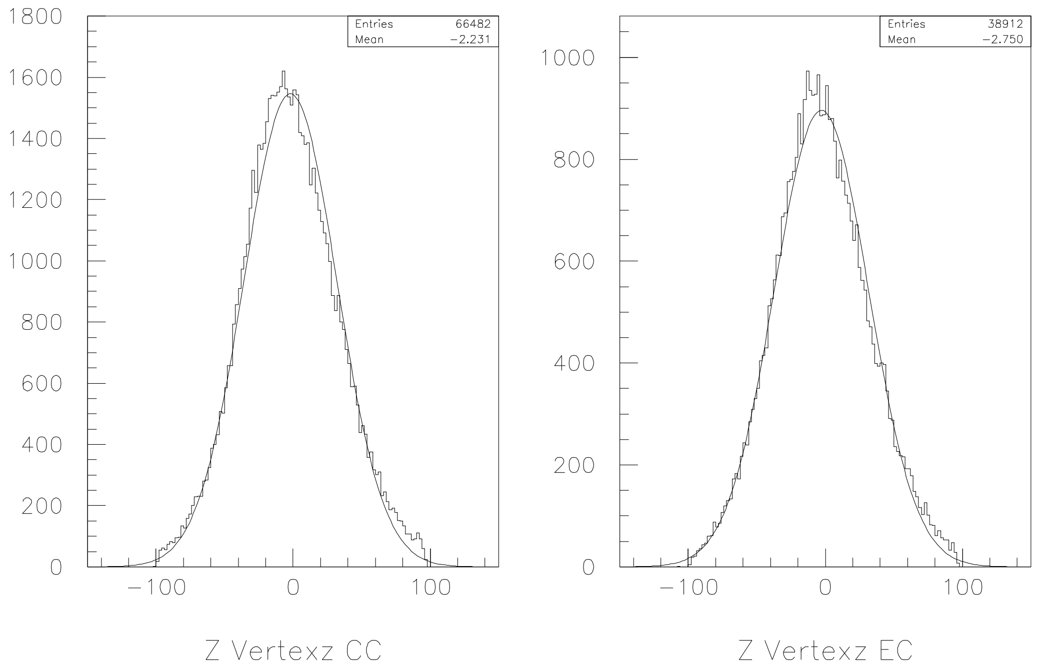

Figure 6: Vertex distribution of isolated photon events

3.3 Charged Track Cut

The presence of a charged track near a shower distinguishes electrons from photons. By removing EM objects with an associated charged track extrapolated from the wire chambers, contamination of the photon signal by electrons was greatly reduced. However, this can lead to rejection of signal if a direct photon has converted or has an unrelated overlapping charged track. The effect is more important in the EC due to the higher track density and the larger amount of material for the γ to convert.

The overall tracking efficiency is parameterized as

$$\epsilon_d = (1 - pt)(1 - \psi)$$

where p is the probability that a photon will convert before the tracking chambers, t is the probability that a track in the detector will be reconstructed, and ψ is the probability that a reconstructed track from the underlying event will be found in the tracking road of a good photon.

The parameter p has been determined previously to be 0.095 ± 0.010 (0.386 ± 0.041) for the CC (EC)[2]. To determine the other parameters, we used a sample of $Z^0 \to e^+e^-$ events from Run 1C (at 1.8 TeV) because the number of Z^0 events at 630 GeV was found insufficient. Z^0 events with no jets in the event were chosen to avoid electrons that may have overlapped a jet, and to ensure a topology similar to that of photon events where any jets are generally in the opposite hemisphere from the photon. Both EM clusters where also required to have a reconstructed E_T above 25 GeV.

To determine t, both electrons from the Z^0 decay were requiremed to have:

- $\eta < 0.9$
- At least one track in the road
- Track match significance $\sigma_t < 5$ (10) in the CC (EC).
- EM fraction $> 95\%$
- Isolation fraction $< 20\%$
- Hmatrix $\chi^2 < 100$.

Each EM shower passing these requirements were tagged as a good electron, and the other electron from Z^0 decay was considered unbiased and usable for determining the tracking efficiency. Photon selections, except the tracking cut, were applied to the unbiased sample and any candidate that passed these cuts was checked for $\sigma_t < 5$ (10) in the CC (EC). Invariant mass distributions were calculated for all candidates passing the photon selections, both with and without the tracking criteria. The tracking efficiency was determined by calculating how many electrons from $Z^0 \to e^+e^-$ events passed the tracking requirement. The number of events in the Z^0 signal region (N_S) was determined from events having an invariant mass between 86 and 96 GeV/c^2. The background was defined in two regions on either side of the Z^0 peak from 61 to 71 GeV/c^2 and from 111-121 GeV/c^2, with the number of background events (N_B) being half of the total number in these two regions. Events with and without tracks in the CC and EC are shown in Fig. 7. The tracking efficiency is given by

$$t = \frac{N_{TS} - N_{TB}}{N_S - N_B}$$

where the subscript T indicates the number of events with associated tracks. The tracking efficiency is estimated as $t = .769 \pm .024 \pm .017$ ($.683 \pm .042 \pm .002$) in the CC (EC), where the first error is statistical and the second systematic, the latter estimated by the difference in efficiency with and without background subtraction.

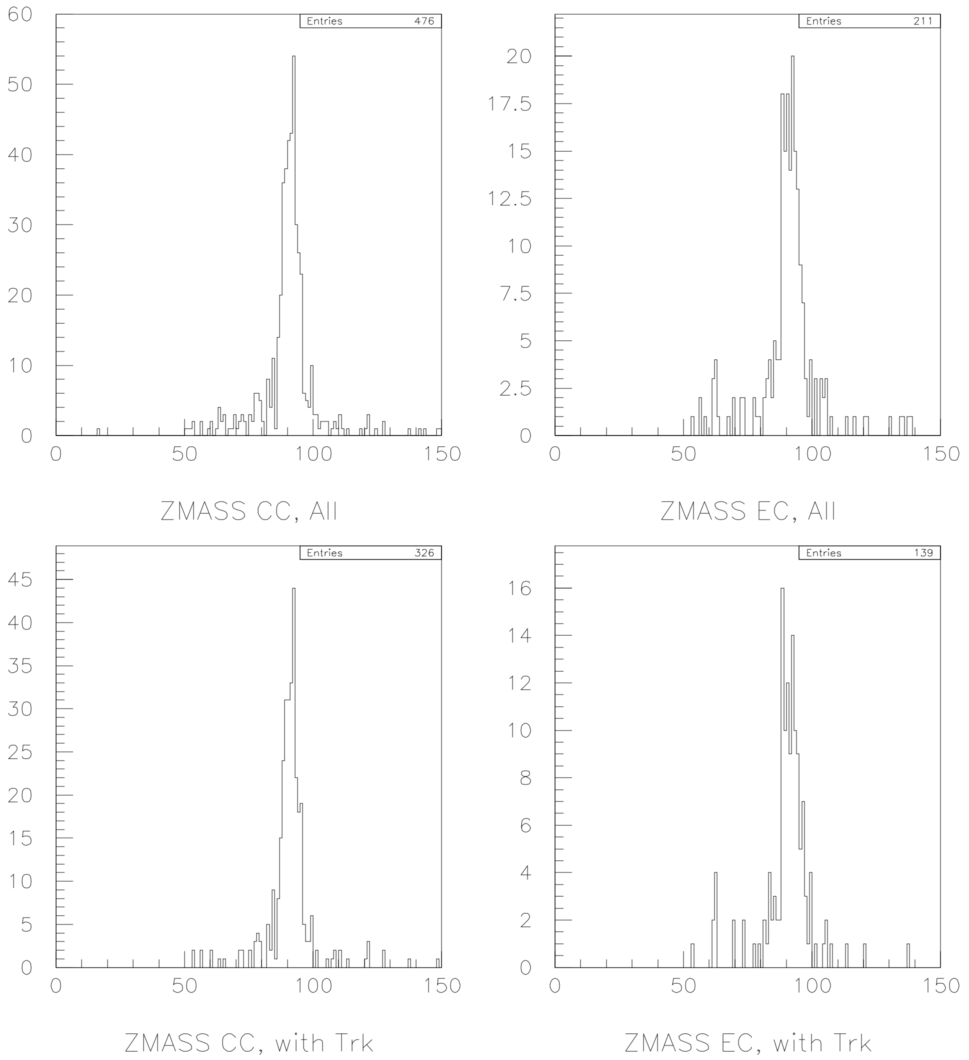

Figure 7: Invariant mass peaks for events with two unbiased EM clusters passing photon selections and for same events also passing electron tracking requirements in the CC and EC.

The track overlap probability, ψ, was obtained using the same method described above for determining t, but with an additional track in the road pointing to the EM cluster. The estimated track overlap probability is $\psi = .074 \pm .014 \pm .008$ ($.195 \pm .033 \pm .044$) in the CC (EC), where the first error is statistical and the second is systematic. The systematic uncertainty is estimated from a comparison of two different methods used in the Run 1A analysis to determine ψ. One of the methods is the same as used in this analysis, and the other uses very clean photons and any tracks in the road pointing to the cluster[3]. The percent difference between the two methods for the Run 1A analysis was used as the systematic uncertainty in this analysis.

Combining the values for p, t, and ψ, the total tracking efficiency is found to be $\epsilon_d = 0.858 \pm 0.018$ (0.593 ± 0.079) in the central (forward) region.

3.4 Selection Cuts

The selections listed in Section 2.3 are applied to remove most of the multi-particle background. The isolation, EM fraction, and H-matrix χ^2 cuts select EM objects consistent with being single particle showers.

For the Run 1A analysis [1] and for Jerger's thesis [3], the fully simulated photon events were used to determine selection efficiencies. For the new combined Run 1A/B analysis, the larger data set of single photons was used [4]. For energies above 10 GeV, these two efficiencies are comparable, but for lower energies, they are very different, as shown in Fig. 8. Because there is no *a priori* reason to expect that either method gives the better result, the average of the two methods is used, and the difference from the average is taken as a systematic uncertainty. A fuller discussion on how the MC simulation of efficiencies was verified at 40 GeV, using electrons from W decay, can be found in References [2, 3].

4 Photon Purity

4.1 Purity Determination

The isolated direct photon sample is contaminated with a background arising from jets that have fluctuated into isolated EM objects. It consists mainly of isolated π^0 or η mesons (from jets), which decay into two photons not resolved because of the calorimeter granularity. This background cannot be singled out on an event by event basis, and is corrected instead in each E_T region

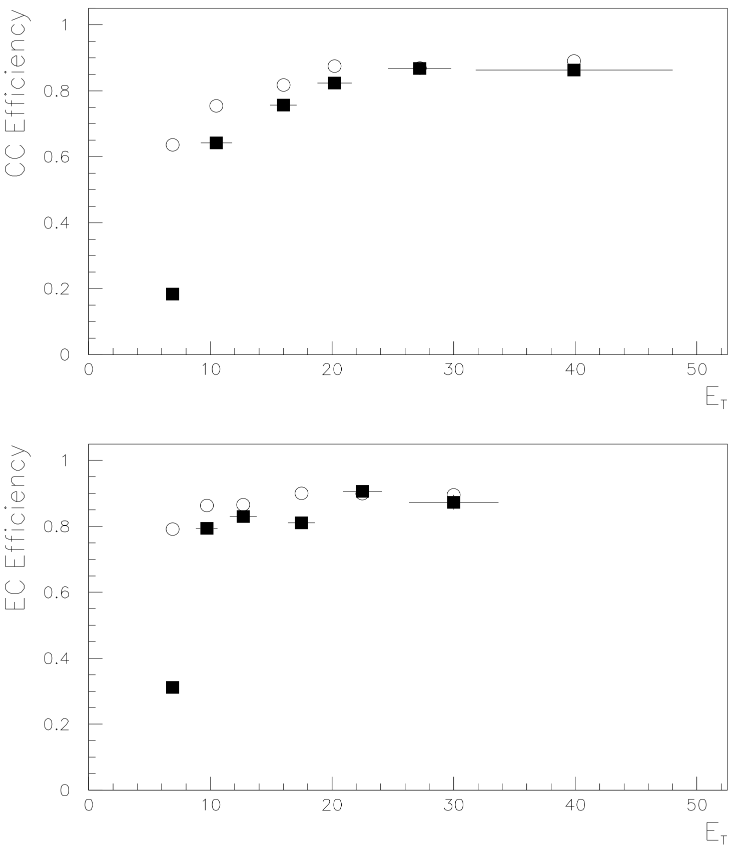

Figure 8: Selection efficiencies for the central and forward η regions. The squares use the full Monte Carlo with fewer events while the circles use the single-photon Monte Carlo, only simulating the event in an $R = 0.7$ cone around the photon.

by means of an average photon fraction, or purity ($\mathcal{P}$), defined as the ratio $\mathcal{P} = \gamma/(\gamma+\text{jet})$, where γ and jet, respectively, correspond to the number of direct photons and background jets that survive the selection criteria.

The photon purity is estimated by comparing the distributions of different observables in the data with MC predictions for photons and jets. Variables sensitive to the difference between single and multi-photon showers, and well reproduced by the MC simulation, are particularly suitable for this analysis. Following analyses in Run 1A and Run 1B, we investigated the fraction of energy deposited in the first layer of the EM calorimeter (E_1). Single photon showers are less likely to convert early, and thus deposit a smaller E_1 fraction on average. The quantity $\log(E_1/E_{total})$ is used to enhance the sensitivity to the small E_1/E_{total} region, where the difference between single and multi-photon events is largest. Tables 2 and 3 list the number of available MC events.

Fig. 9 presents the data vs. $\log(E_1/E_{total})$ for the central region of rapidity E_T bins of 6–8, 8–13, 13–18, 18–23, 23-33, and >33 GeV, together with MC contributions from photons and jets. The Monte Carlo distributions were fitted to the data using the HBOOK routine HMCMLL, which correctly incorporates statistical errors in both the data and the MC histograms. The mean photon fraction is then obtained by fitting the data to a combination of photons and jets.

For the forward region, the MC distributions have a global offset in $\log(E_1/E_{total})$ with respect to the data, which has been shown to be due to incorrect sampling fraction used in the simulation [2, 3]. This offset was studied extensively in the Run 1B data, and shown to correspond to an additive offset of 0.120 ± 0.011 in $\log(E_1/E_{total})$. A comparison of the mean E_1 of Run 1B and Run 1C before and after imposing selection requirements, is shown in Figs. 10 and 11. Except for high transverse energies in the EC before selections, there is good agreement between the two data sets. Since the correction is applied after cuts, and since most of the photons lie below 20 GeV, the correction determined from Run 1B is applied as a horizontal displacement to the MC in the plot of $\log(E_1/E_{total})$.

Figure 12 presents the EC data vs. $\log(E_1/E_{total})$. The routine HMCMLL is used, and the purity is determined from the same fit as that used in the CC.

To study systematic errors introduced in determining the photon purity, we also performed a fit of Monte Carlo to data with the same fitting function, but using the method described in the Run 1A publication [1], and in Jerger's thesis [3]. This method first uses the HBOOK algorithms to smooth the Monte Carlo distributions, then fits the distributions in the range

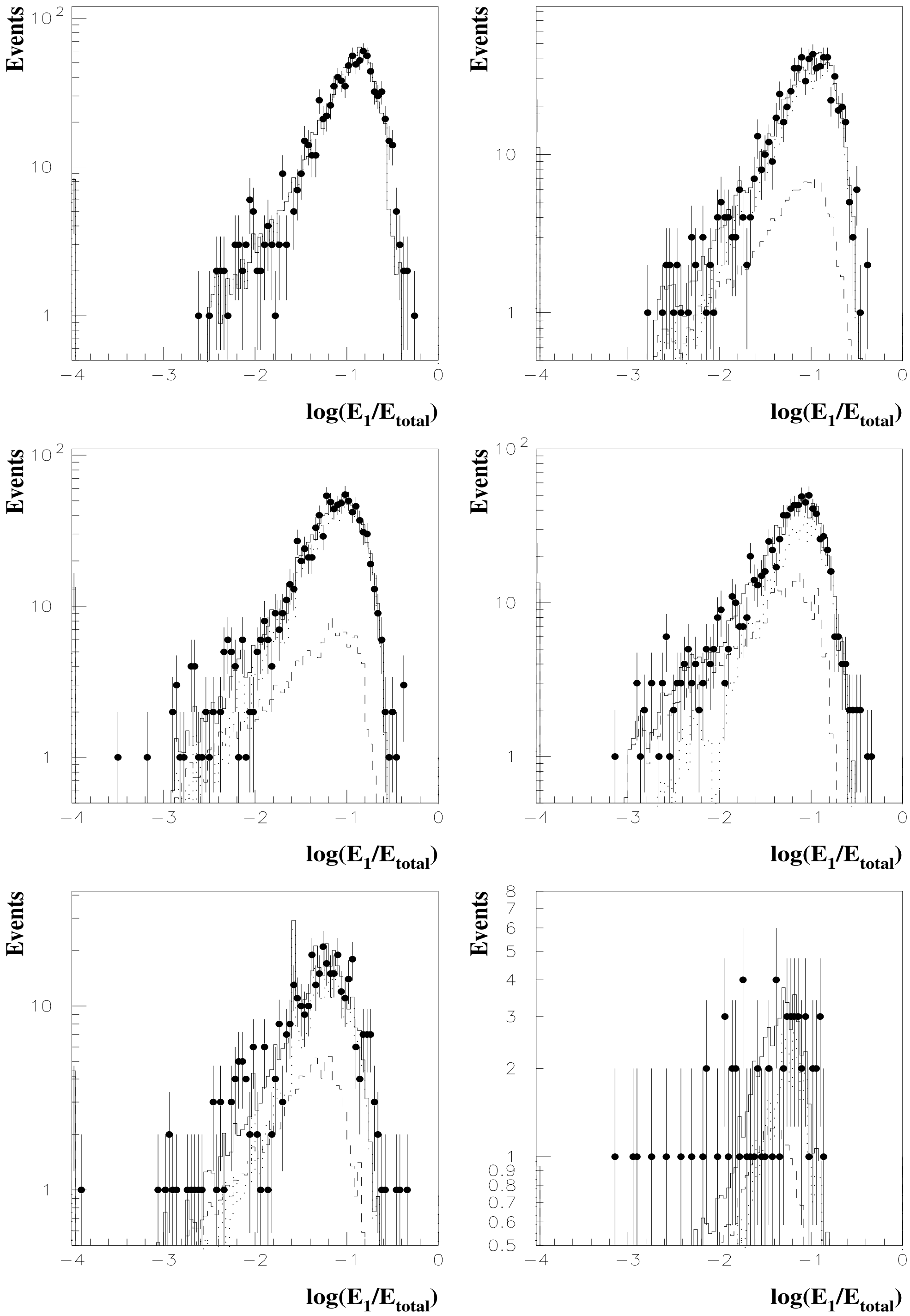

Figure 9: Distributions of $\log(E_1/E_{total})$ for the central $/eta$ region in E_T bins of 6–8, 8–13, 13–18, 18–23, 23–33, and >33 GeV. The solid line is total MC fit to the data. The dashed line is the photon contribution, and the dotted line is the background contribution.

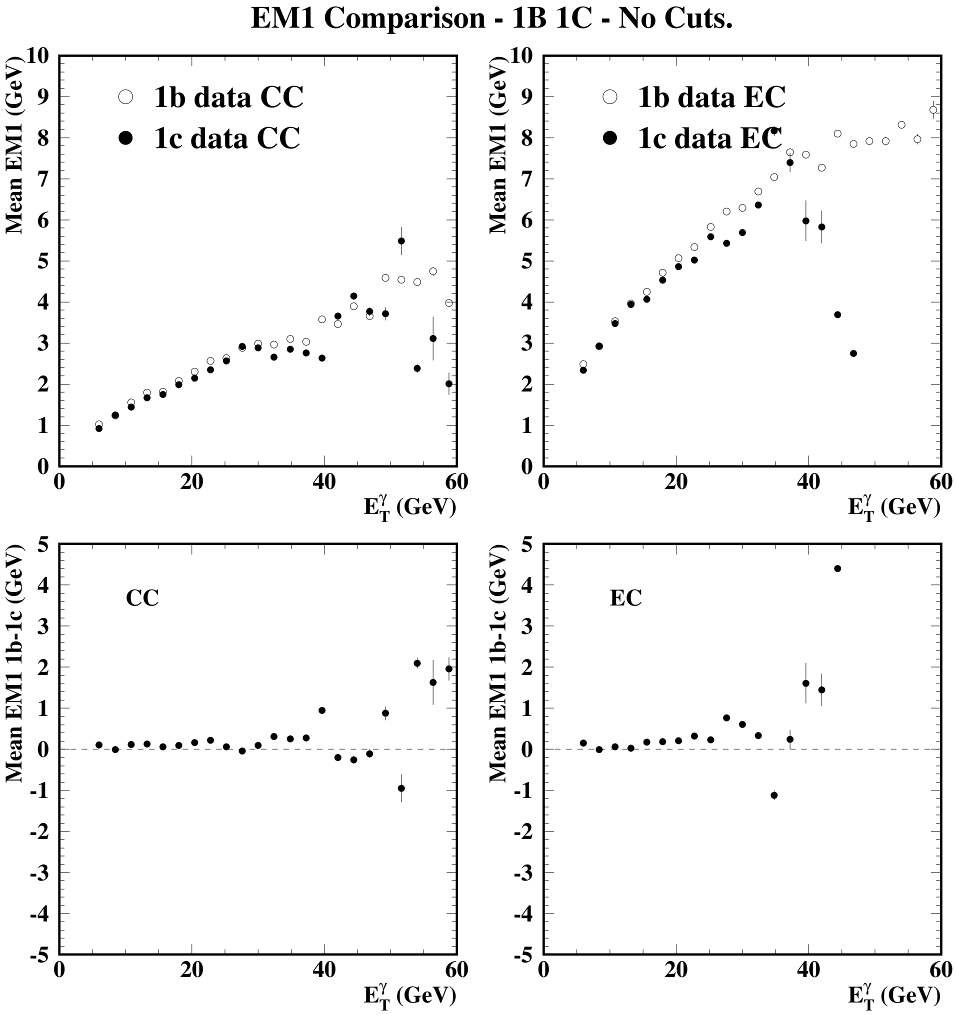

Figure 10: Comparison of E_1 energy for Run 1B and Run 1C, before imposing photon selection criteria.

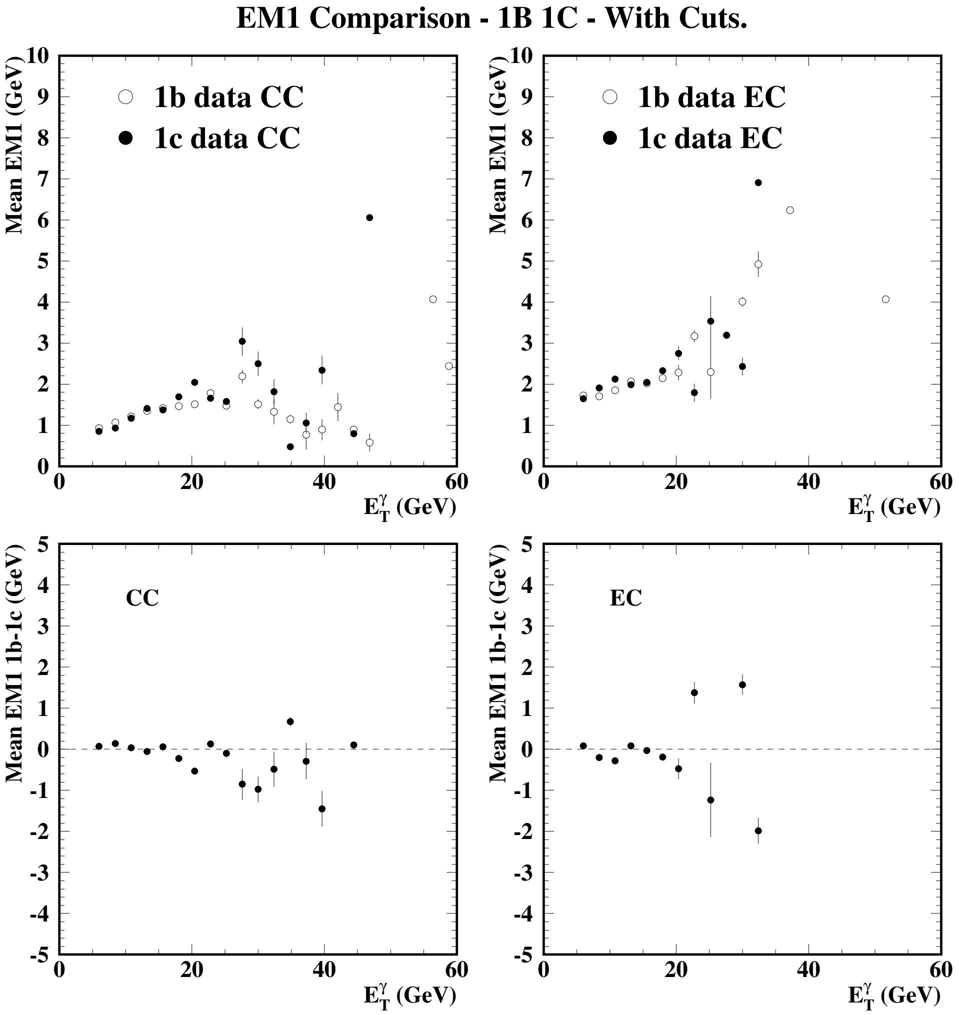

Figure 11: Comparison of E_1 energy for Run 1B and Run 1C, after imposing photon selection criteria.

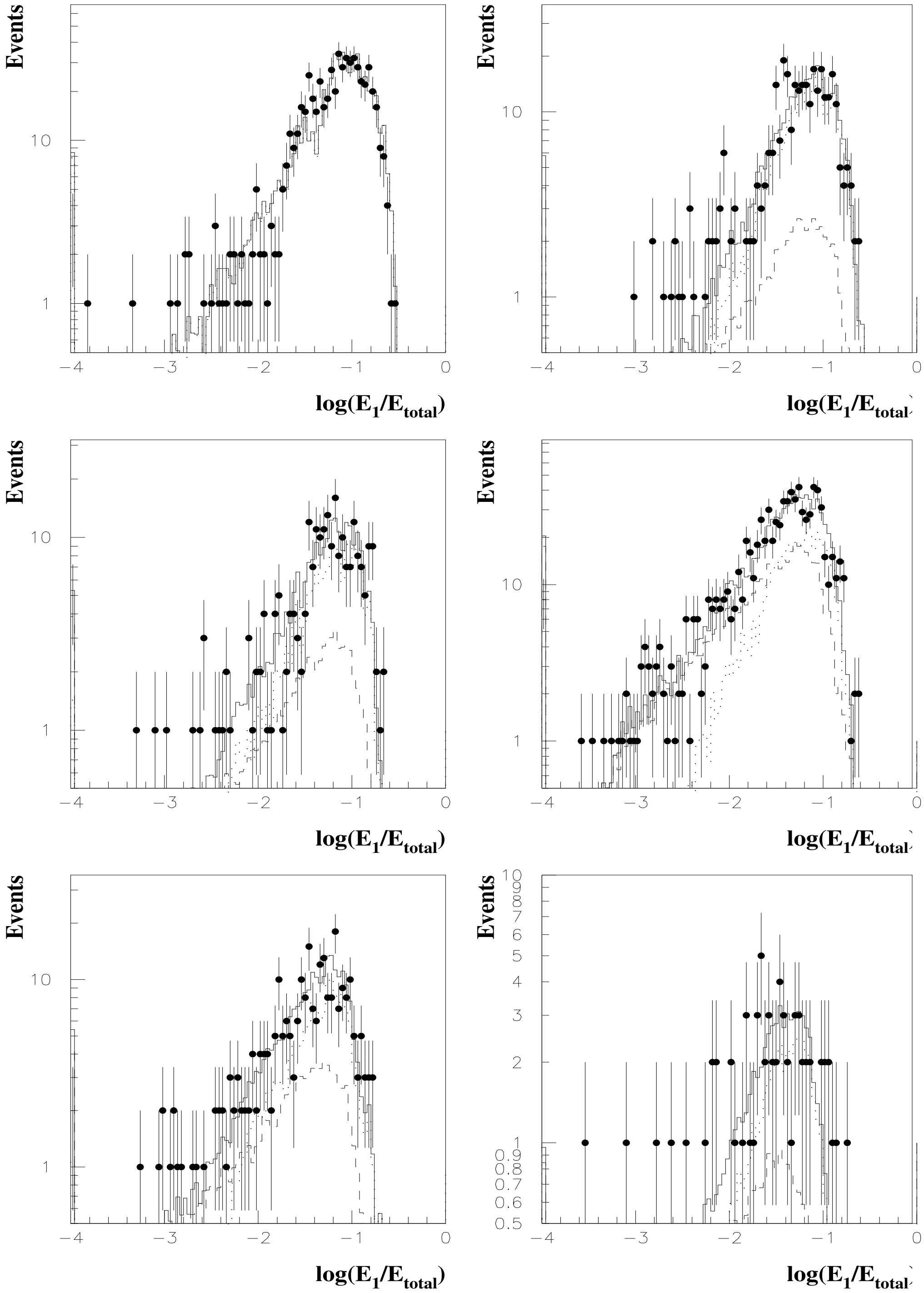

Figure 12: Distributions of $\log(E_1/E_{total})$ for the forward η region in E_T bins of 6–8, 8–11, 11–15, 15–20, 20–26, and >26 GeV. The solid line is total MC fit to the data. The dashed line is the photon contribution, and the dotted line is the background contribution.

$-3.8 < \log(E_1/E_{total}) < -0.6$. The difference between the two methods is summarized in Tables 5 and 6, and is added to the uncertainty in the purity systematics. For further discussion of photon purity, see Appendix A.

E_T Range (GeV)	E_T(GeV)	HMCMLL Fit	Run 1A Fit
6- 8	6.9 ± 0.5	0.0 ± 3.0	0.0 ± 5.3
8-13	10.5 ± 1.3	20.8 ± 5.3	14.8 ± 6.3
13-18	16.0 ± 1.1	18.2 ± 4.5	9.4 ± 4.8
18-23	20.2 ± 1.4	38.1 ± 4.5	32.2 ± 4.9
23-33	27.2 ± 2.6	30.9 ± 6.5	37.5 ± 7.7
>33	39.9 ± 8.1	46.7 ± 14.6	69.8 ± 20.6

Table 5: Results for photon purity in the CC, using the fitting methods described in the text.

E_T Range (GeV)	E_T(GeV)	HMCMLL Fit	Run 1A Fit
6- 8	6.9 ± 0.5	1.5 ± 7.8	5.5 ± 8.8
8-11	9.7 ± 0.9	21.0 ± 8.7	55.9 ± 12.4
11-15	12.7 ± 1.1	30.5 ± 9.6	31.2 ± 15.2
15-20	17.5 ± 1.1	52.8 ± 6.0	53.2 ± 5.2
20-26	22.5 ± 1.6	37.2 ± 10.5	58.9 ± 14.1
>26	30.0 ± 3.7	34.6 ± 14.8	78.7 ± 26.3

Table 6: Results for photon purity in the EC, using the fitting methods described in the text.

4.2 E_T Dependent Fit

The photon fractions were combined with the selection efficiencies (calculated under the same binning) and fitted vs. E_T using a two-parameter functional form:

$$\mathcal{P}/\epsilon_s = \frac{1}{1 + a(E_T)^b}.$$

The fit, shown in Fig. 13. assures that $\mathcal{P}/\epsilon_s$ is a smooth function of E_T. This functional form is chosen because it satisfies the boundary conditions of low purity at low E_T and high purity at high E_T, and because we expect the data to be a sum of two falling cross sections (photons and jets) roughly of the form aE_T^b.

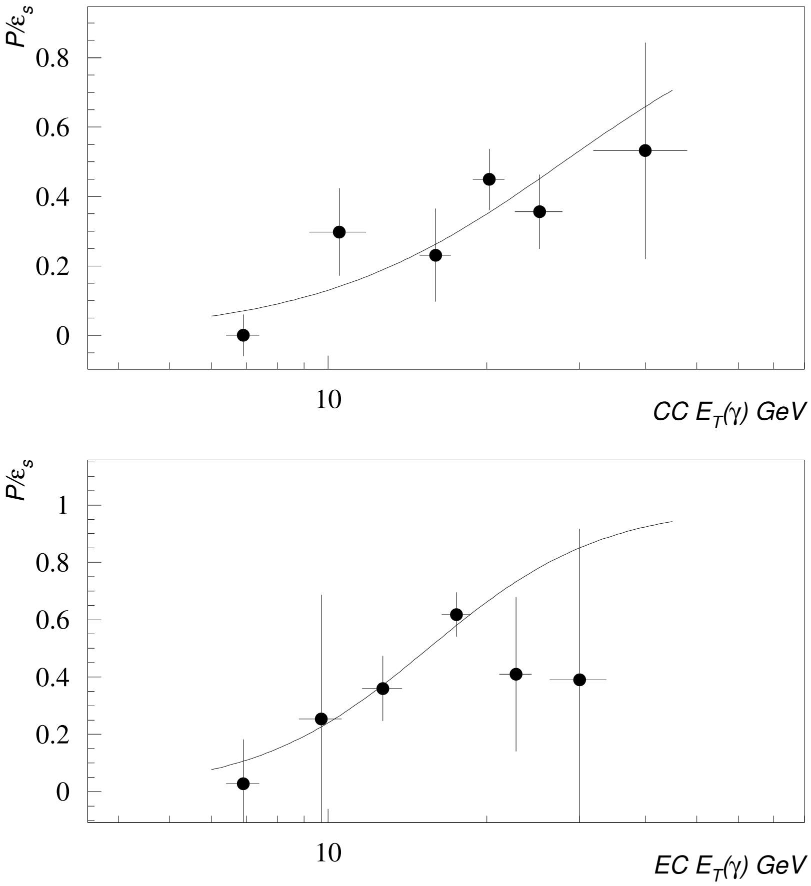

Figure 13: Photon purity for the central and forward regions.

In order to estimate the uncertainty from our choice of E_T binning and fitting function, we have used three alternative functions to fit the data, and two other choices of E_T binning. The alternative fitting functions are

$$\mathcal{P}/\epsilon_s = 1 - e^{-(a+bE_T)},$$

$$\mathcal{P}/\epsilon_s = a + bE_T,$$

and

$$\mathcal{P}/\epsilon_s = a + b\log E_T.$$

The results of these alternative fits are shown in Tables 7 and 8 and Figs. 14-16.

E_T **Bins**	Fit	**Fitting Functions**			
		$\frac{1}{1+ax^b}$	$1-e^{-(a+bx)}$	$a+bx$	$a+b\log x$
6-8-13-	a	469 ± 499	$-.19 \pm .10$	$-.099 \pm .008$	$-.60 \pm .18$
18-23-33	b	$-1.8 \pm .36$	$.032 \pm .008$	$.022 \pm .005$	$.33 \pm .07$
6-7-10-	a	151 ± 110	$-.069 \pm .090$	$-.032 \pm .081$	$-.38 \pm .17$
16-20	b	$-1.3 \pm .24$	$.018 \pm .005$	$.014 \pm .004$	$.21 \pm .06$
6-8-11-	a	825 ± 796	$-.20 \pm .12$	$-.10 \pm .12$	$-.64 \pm .25$
15-20-26	b	$-2.1 \pm .32$	$.032 \pm .008$	$.023 \pm .006$	$.34 \pm .09$

Table 7: Fitting the Purity in the central region, using different functions and different binning with $x = E_T$.

E_T **Bins**	Fit	**Fitting Functions**			
		$\frac{1}{1+ax^b}$	$1-e^{-(a+bx)}$	$a+bx$	$a+b\log x$
6-8-13-	a	36 ± 59	$-.008 \pm .319$	$.13 \pm .21$	$-.35 \pm .48$
18-23	b	$-1.3 \pm .62$	$.042 \pm .025$	$.021 \pm .014$	$.31 \pm .18$
6-7-10-	a	1420 ± 2459	$-.39 \pm .15$	$-.19 \pm .13$	$-.88 \pm .26$
16-20	b	$-2.5 \pm .63$	$.063 \pm .015$	$.038 \pm .009$	$.48 \pm .11$
6-8-11-	a	1352 ± 4083	$-.49 \pm .25$	$-.12 \pm .20$	$-.98 \pm .45$
15-20-26	b	-2.6 ± 1.1	$.077 \pm .020$	$.038 \pm .013$	$.54 \pm .17$

Table 8: Fitting the Purity in the forward region, using different functions and different binning with $x = E_T$.

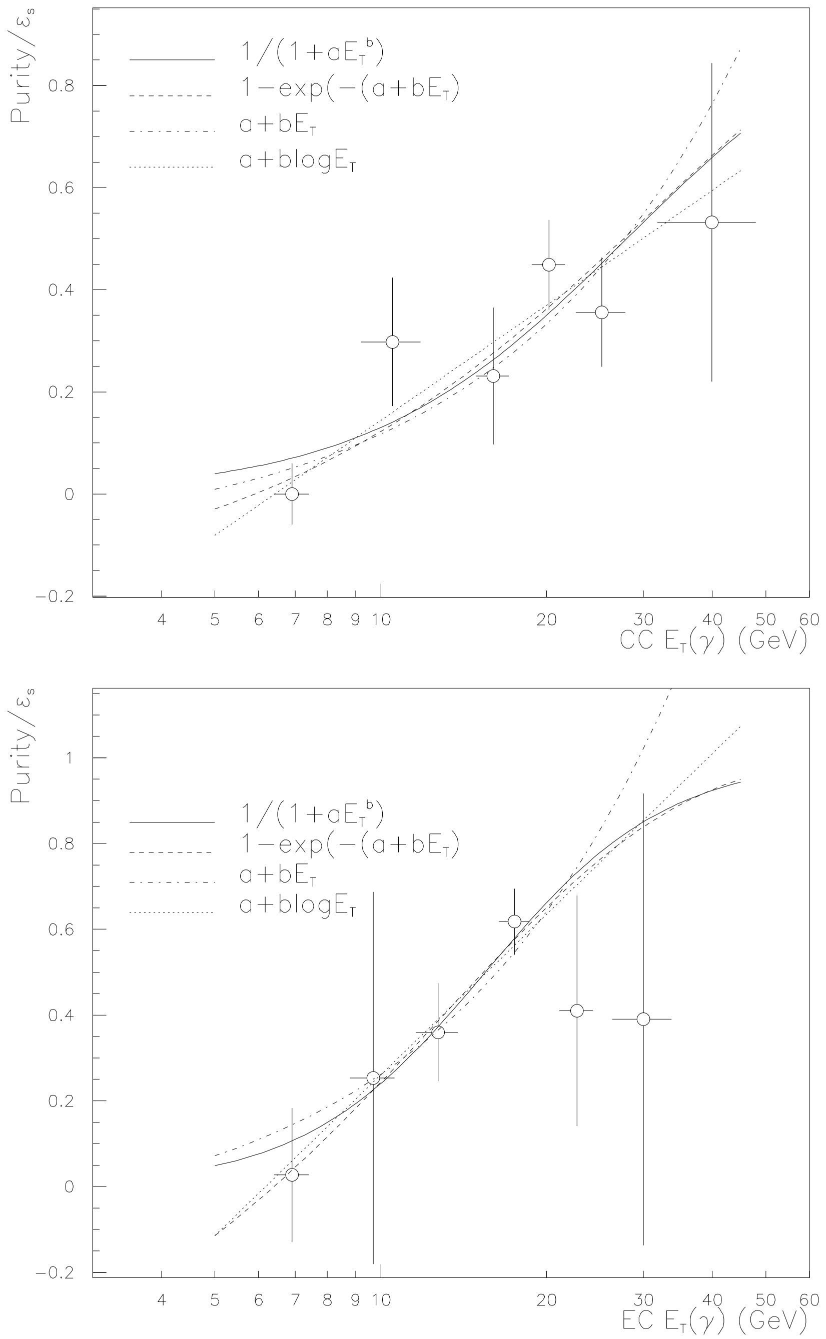

Figure 14: $\mathcal{P}/\epsilon_s$ using different fitting functions (a) CC and (b) EC.

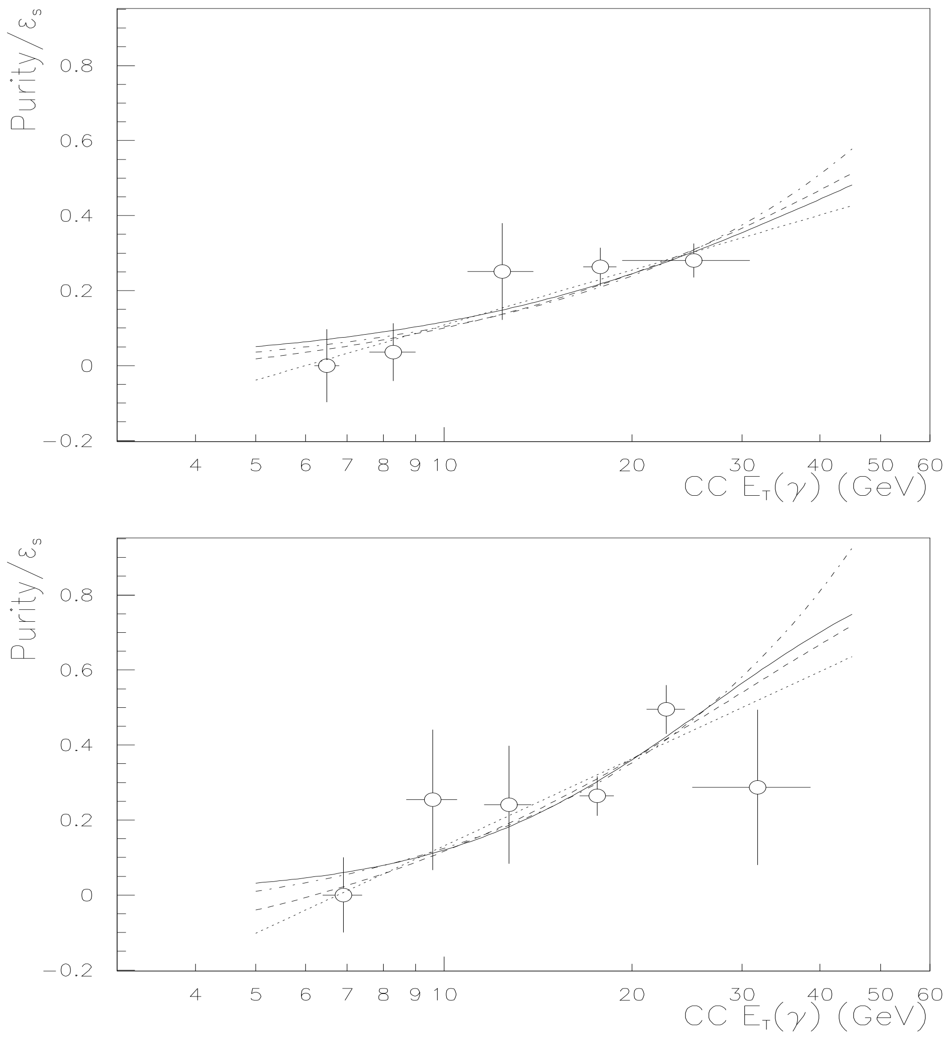

Figure 15: $\mathcal{P}/\epsilon_s$ with alternative E_T bins and four different fitting functions in the central rapidity region. The legend is the same as in Fig. 14.

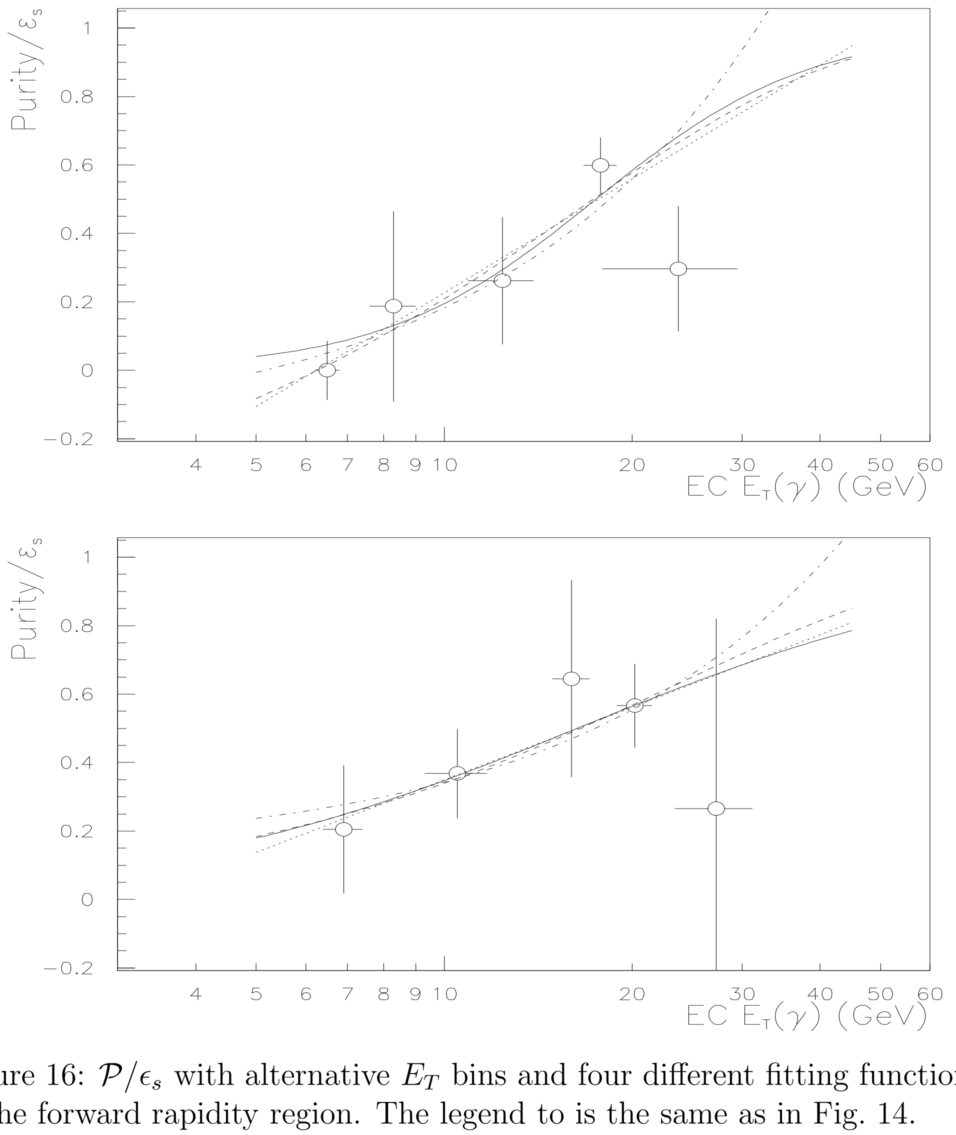

Figure 16: $\mathcal{P}/\epsilon_s$ with alternative E_T bins and four different fitting functions in the forward rapidity region. The legend to is the same as in Fig. 14.

Except for in the high E_T regions, a comparison of the fit parameters in Tables 7 and 8, and the curves in Figs. 14-16 indicate that the spread on all of the alternative fits for different binning is smaller that the individual errors on the data points. The systematic uncertainty is determined by calculating the rms value of the different fits and different binning from the default choices. In Fig. 17, we have plotted the systematic band in uncertainty determined from the rms, the fits with the largest excursions using all of the alternative fits and binning, and the default fit.

5 Cross Sections and Comparison to Theory

Using the selections, efficiencies and photon purity determinations discussed in the previous sections, we can evaluate the cross section using equation 1. If an event had more that one photon candidate, the two more energetic ones were selected, and the selection criteria applied to each separately. Table 9 shows the number of candidates surviving each step. The last cut, indicated as Filter, selects only those events in which the energy of the photon candidate is in the same energy range as the trigger that fired the event.

	$\|\eta\| < 0.9$		$1.6 < \|\eta\| < 2.5$	
Cut	Number of candidates	Lost events %	Number of candidates	Lost events %
Initial	64809	–	37960	–
$E_T > 6.0$ GeV	28239	56.4	20583	45.8
Vertex	23803	15.7	17304	15.9
$\eta^{det} + \phi$ crack	18378	22.8	16286	5.9
Track Veto	11486	37.0	6566	59.6
EM Fraction	9521	17.1	6293	4.2
χ^2	6553	31.2	4074	35.3
Isolation	5807	11.4	3884	4.7
Filter	3926	32.4	2294	40.9
Final Sample	**3926**	**93.9**	**2294**	**94.0**

Table 9: Number of photon candidates after each selectrion step for the CC and EC data.

The number of events satisfying the selections divided by the luminosity, are shown as a fundtion of E_T in Figure 18 for the central and forward regions.

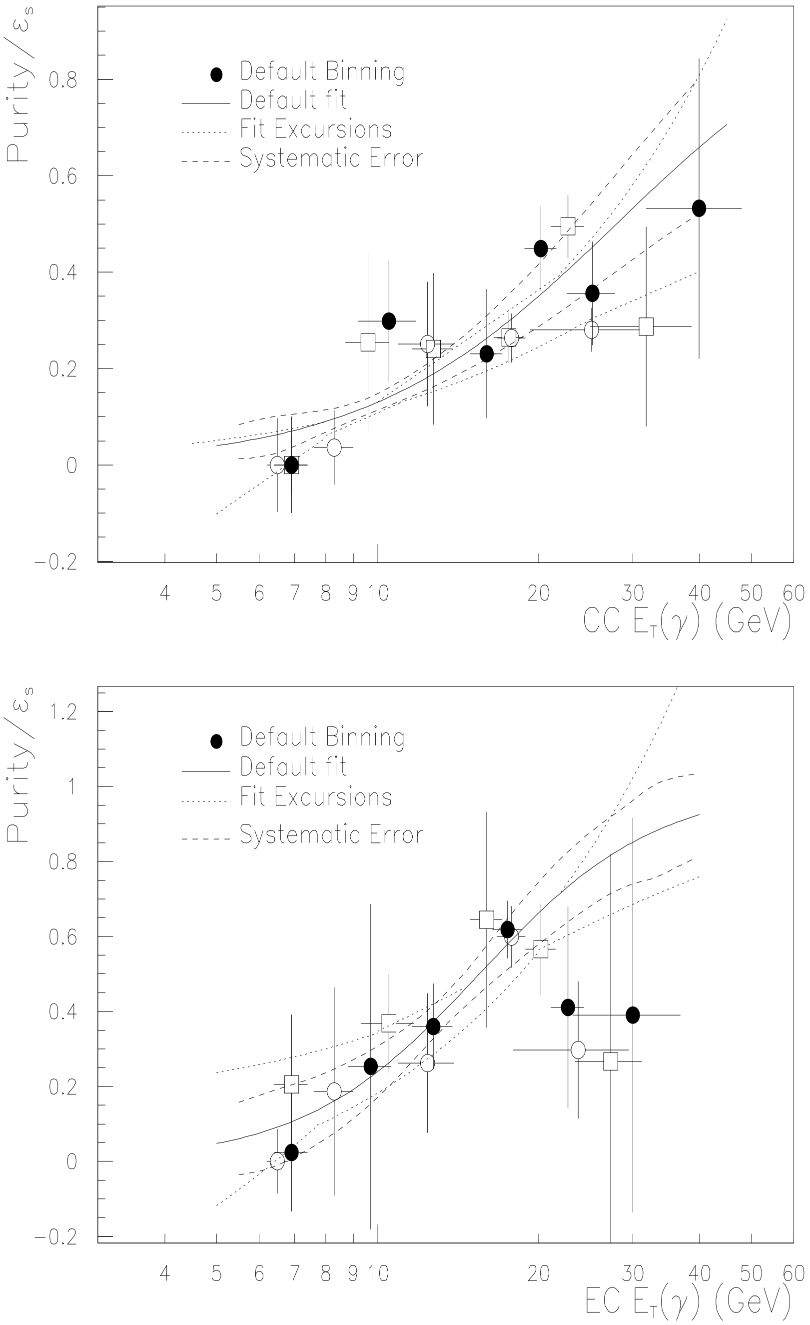

Figure 17: Band in systematic uncertainty and maximum excursion from four possible fitting functions and three different bin selections for CC and EC data.

Figure 19 displays the isolated photon cross sections for the central and forward rapidity regions, together with the theoretical prediction from Owens, Baer and Ohnemus [11], using the CTEQ4M parton distribution functions, smeared with DØ photon energy resolutions. Figure 20 compares the data to the theoretical prediction in terms of the quantity (Data-theory)/Theory. Although these plots show the current version of CTEQ4 as run by Steve Linn, there seems to be a discrepency between these version of CTEQ4 and an earlier version used in the original analysis of this data in 1997. Figure 21 shows a comparison between the current theory and the theory used in 1997 for the central rapidity region.

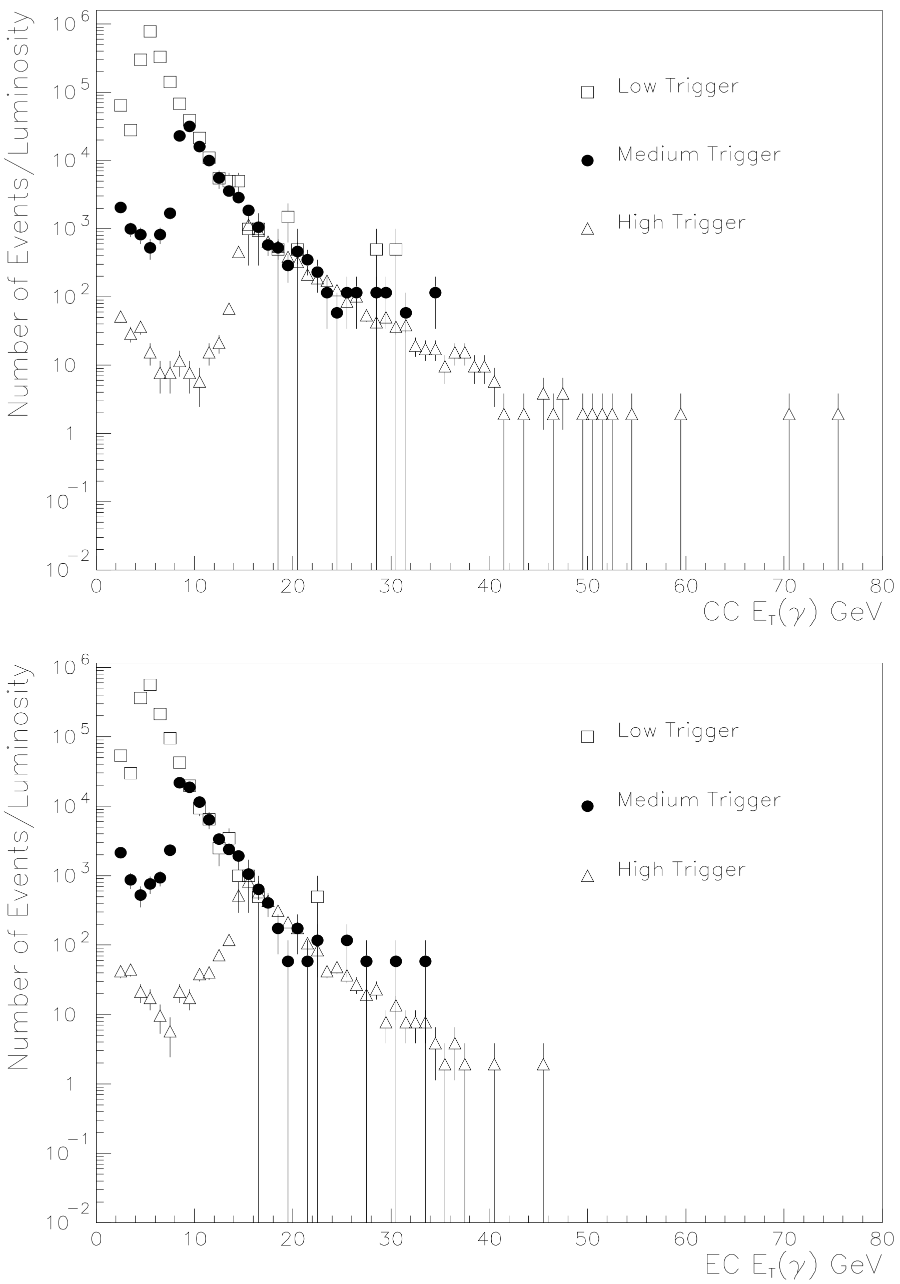

Figure 18: Luminosity-corrected yields for the central and forward region as a fundtion of E_T.

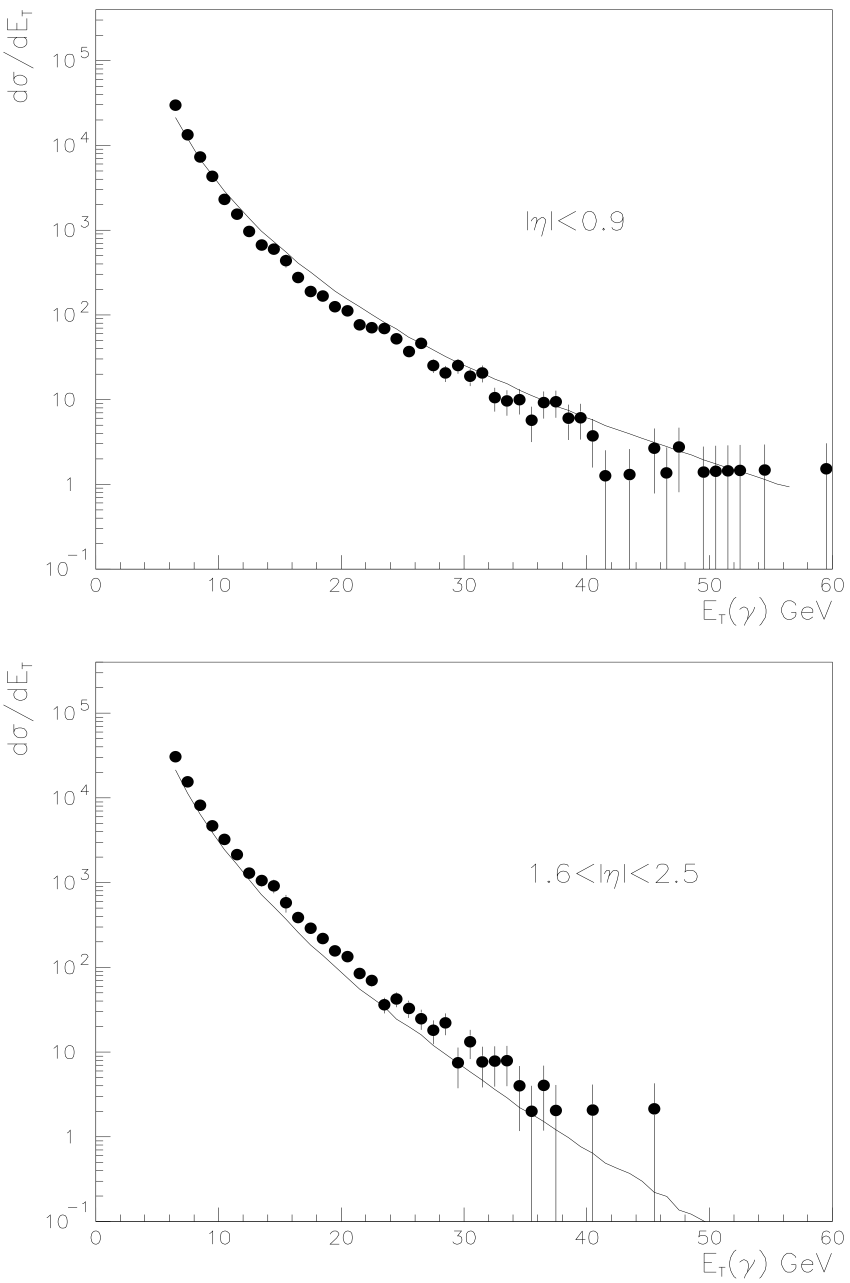

Figure 19: The isolated photon cross section, $d\sigma/dE_T\ d\eta$, vs. photon E_T for the central and forward rapidity regions. The errors arestatistical.

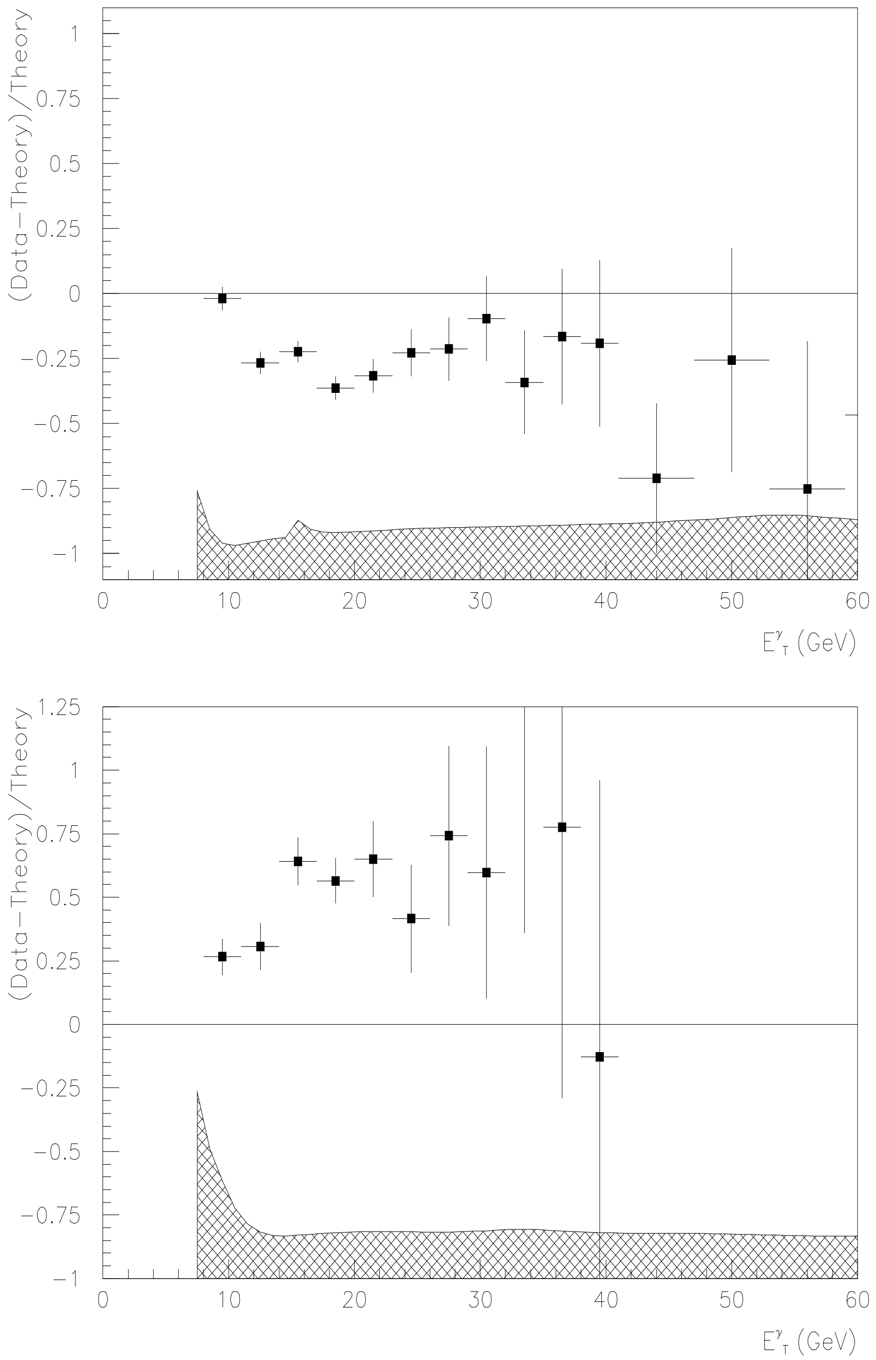

Figure 20: (Data-Theory)/Theory for the central (top) and forward (bottom) rapidity regions. The hatched region shows the systematic uncertainty.

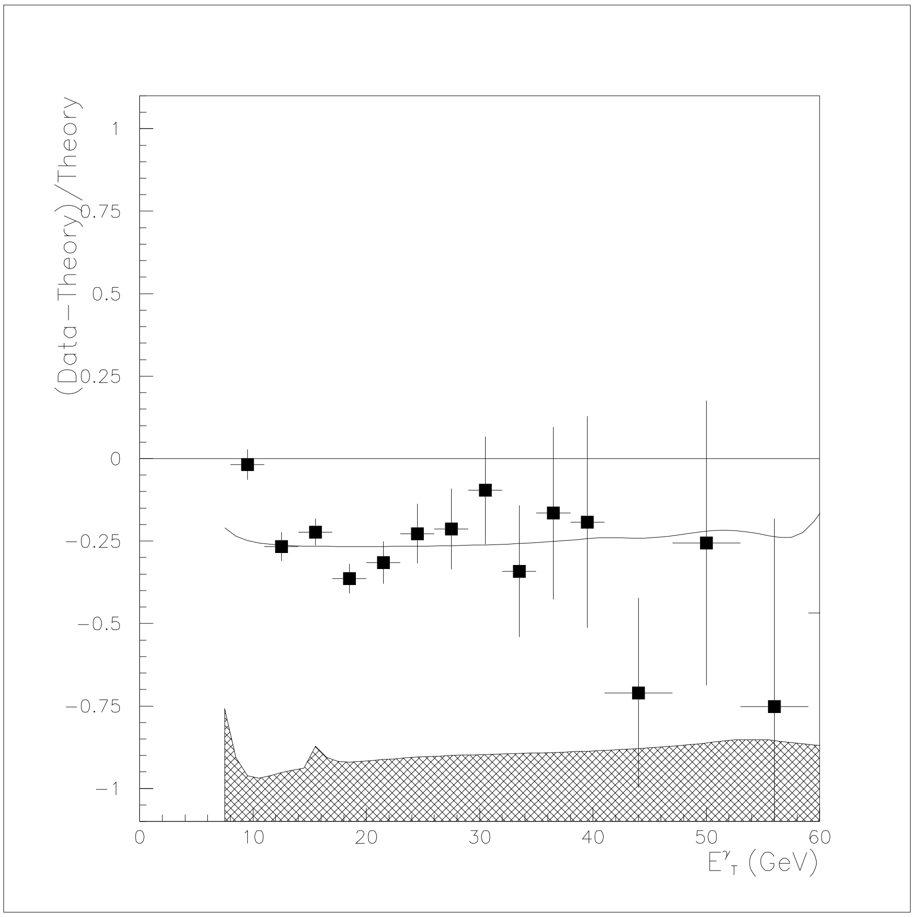

Figure 21: Same plot as Fig. 20, but with the version of CTEQ4 used in 1997 shown as the solid line.

A Extended Studies on Photon Purity

The extended tests in this appendix were performed by fitting the purity distributions in the CC region using smoothed HBOOK Monte Carlo distibutions and MINUIT.

A.1 Monte Carlo Events

It was mentioned in Section 2.2, that the MC statistics were increased by overlaying eight to ten different zero bias events onto the same GEANT event. We have recalculated the photon purities for the central regions, but allowing each Pythia event to be used only once in the analysis. The comparison of results with the enlarged MC sample is summarized in Table 10.

$\boldsymbol{E_T}$**Bin (GeV)**	$\boldsymbol{E_T}$**(GeV)**	**Case A**	**Case B**
8-13	10.6 ± 1.2	14.8 ± 5.70	20.2 ± 5.2
13-18	16.5 ± 1.1	9.4 ± 4.8	12.9 ± 4.5
18-23	19.9 ± 1.4	32.2 ± 4.9	27.8 ± 4.5
23-33	26.3 ± 2.6	37.5 ± 7.7	28.4 ± 7.1
>33	37.6 ± 3.8	69.8 ± 20.6	72.4 ± 25.8

Table 10: Purity results with (case A) and without (case B) several noise files overlayed for the same Pythia event.

A.2 Other discriminant variables: Spread, Isolation, χ^2 and EMF

A large set of variables was investigated as possible discriminants of the photon fraction in the candidate sample. Figs. 22–25 show the results in the central region for four particular choices: the rms spread of the EM object, its isolation, the χ^2 result of the H-Matrix, and the electromagnetic fraction. These variables are compared to a purity fit that used the HBOOK smoothed MC jet and photon distributions.

A jet that has passed all electromagnetic cuts is expected to have a larger mean spread and χ^2, and a higher energy deposition in the isolation cone and in the hadronic part, than a true isolated photon. This is indeed reflected for the first three cases in Figs. 22, 23 and 24, in the comparison of the respective MC photon (dotted line) and jet (dashed line) distributions.

On the other hand, the MC predicted EMF, or fraction of the energy deposited in the first layer of the hadronic calorimeter, is similar for photons and jets. Figure 25, shows the data distributions, together with MC photons and jets normalized to the same number of events. It is clear that both MC distributions are similar, and they describe the data fairly well. The EMF, thus, cannot be used to determine the fraction of photons in the sample.

The extracted photon purities are plotted vs E_T in Fig. 26. For comparison, we have superimposed on the plots the fit and error band obtained using $\log(E_1/E_{total})$ as discriminant variable, fit with the HBOOK smoothing algorithm.

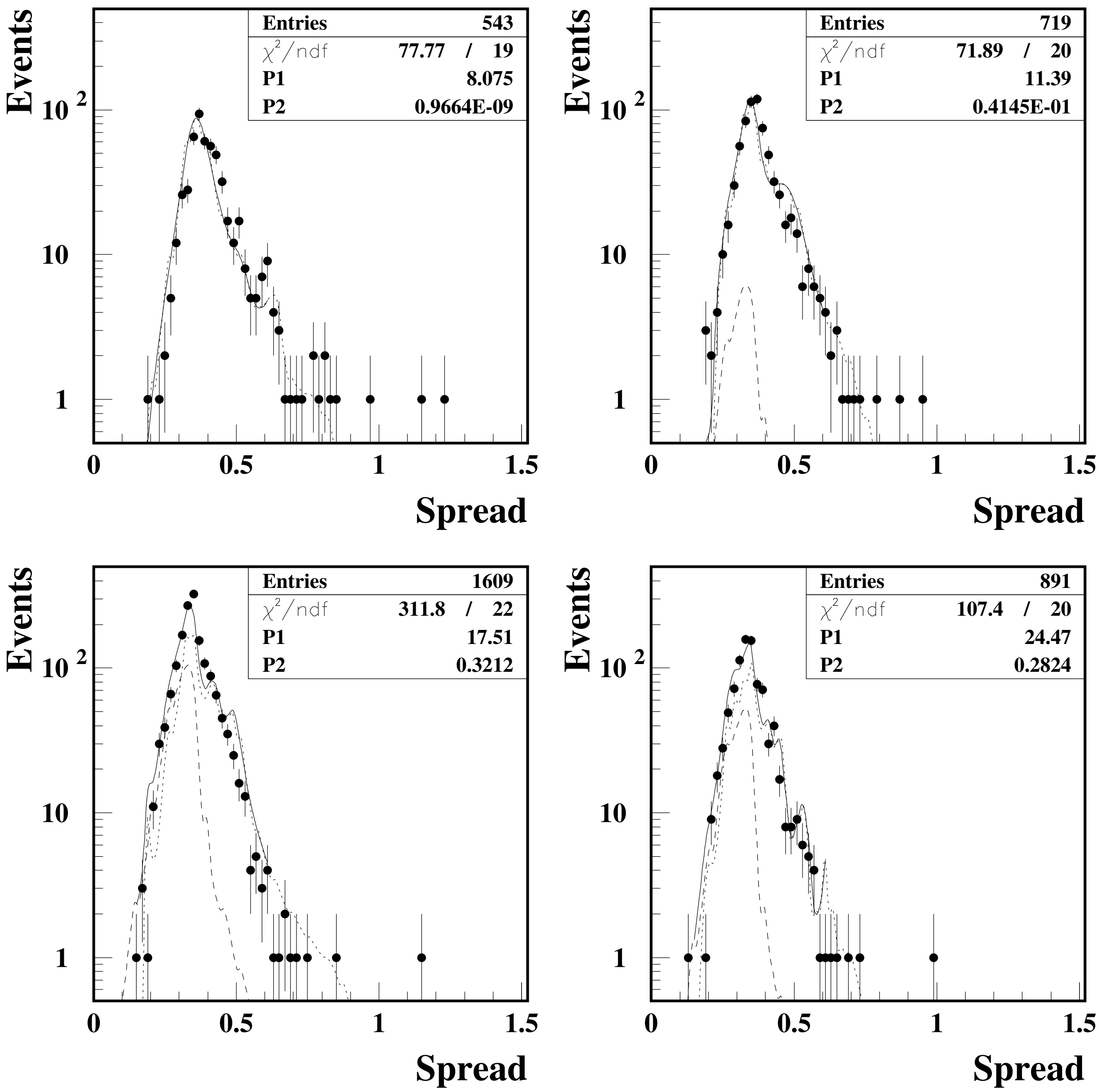

Figure 22: Distribution of rms Spread for the CC showers, in four E_T regions. Solid points are data. Solid, dotted and dashed lines correspond to total fit, MC photons, and MC jets, respectively. P1 is $\langle E_T \rangle$, and P2 the fitted photon purity for each range of E_T .

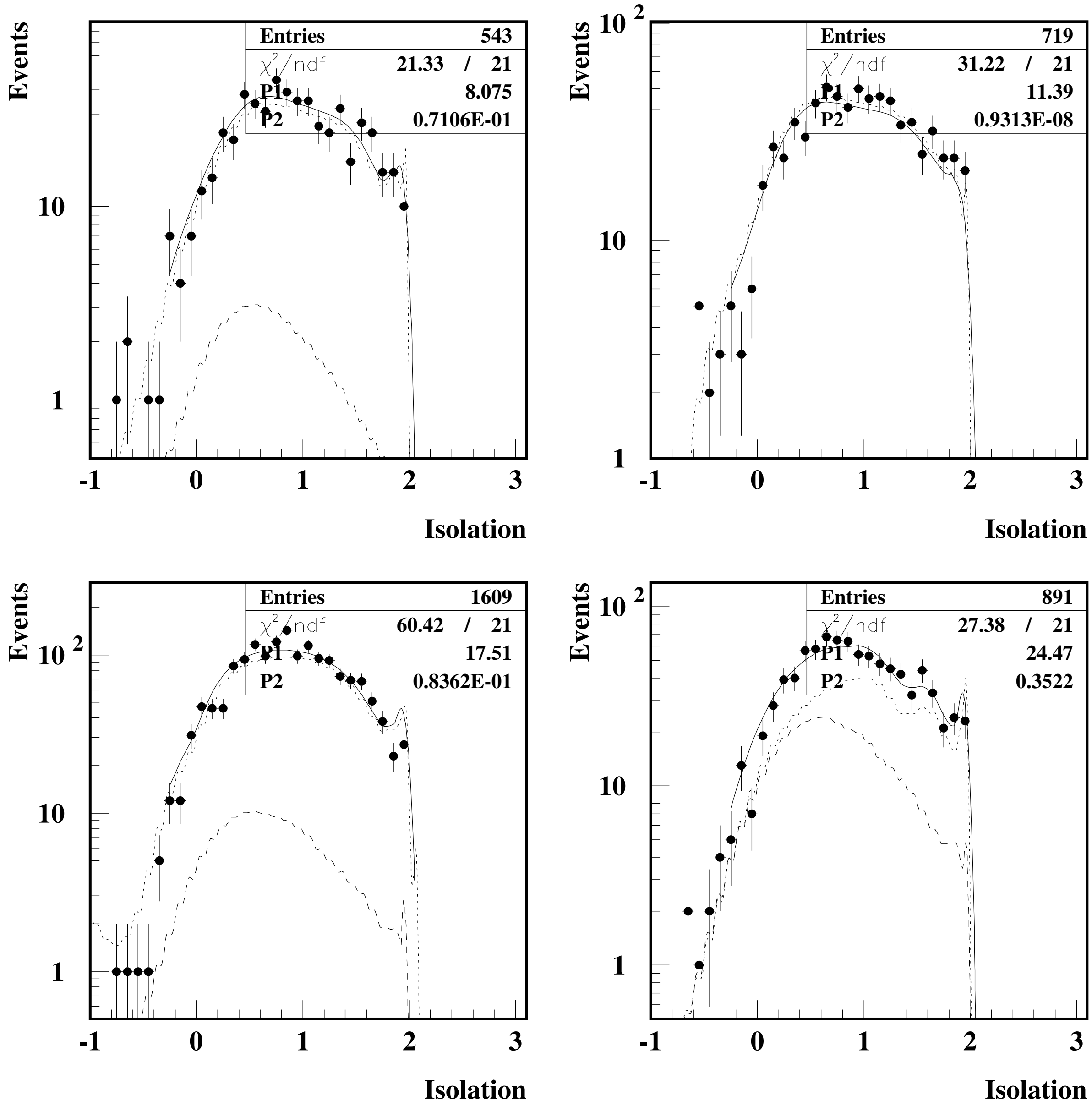

Figure 23: Distributions in the isolation variable for the data in the central region.

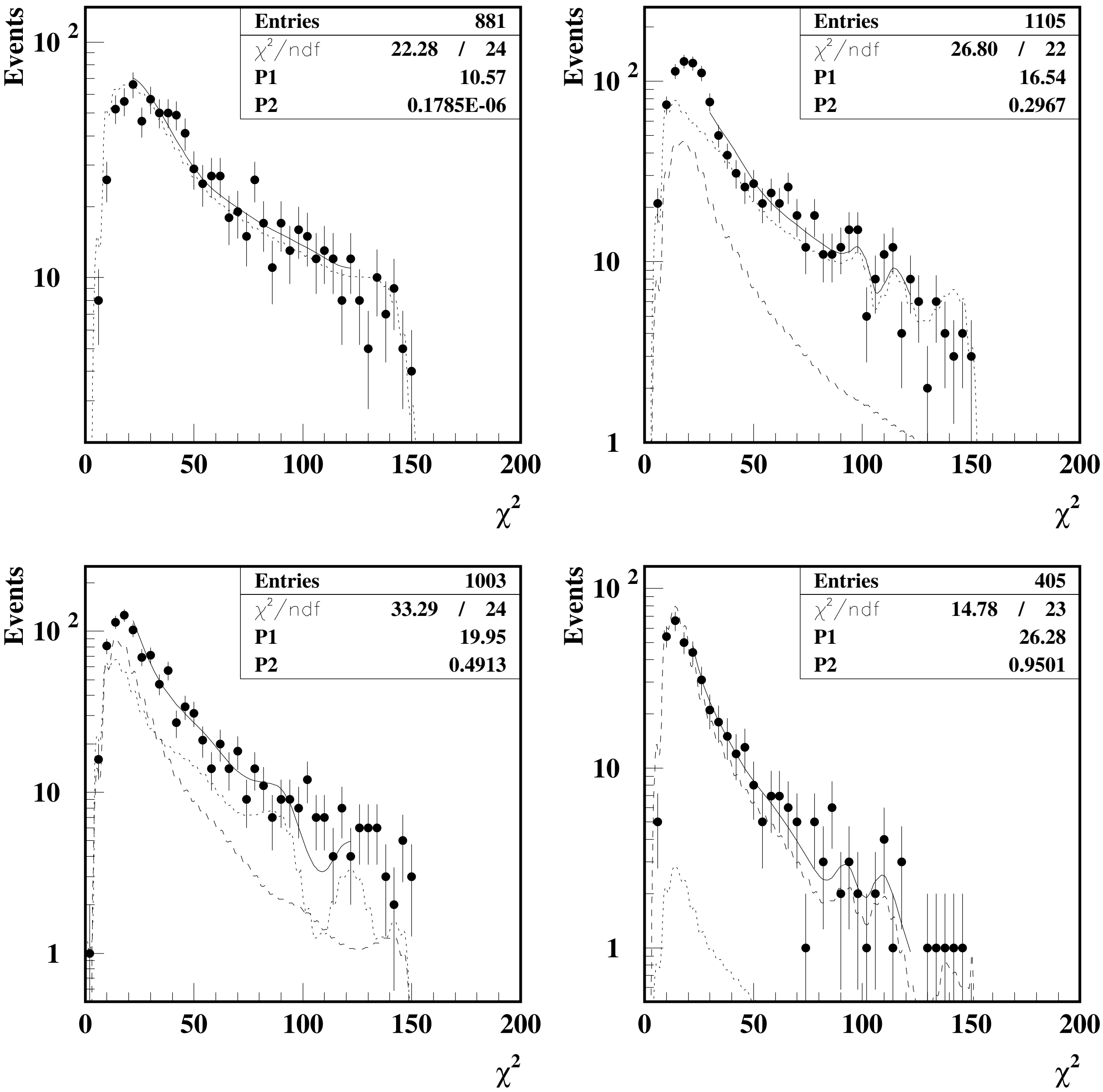

Figure 24: Distributions of χ^2 for the central region.

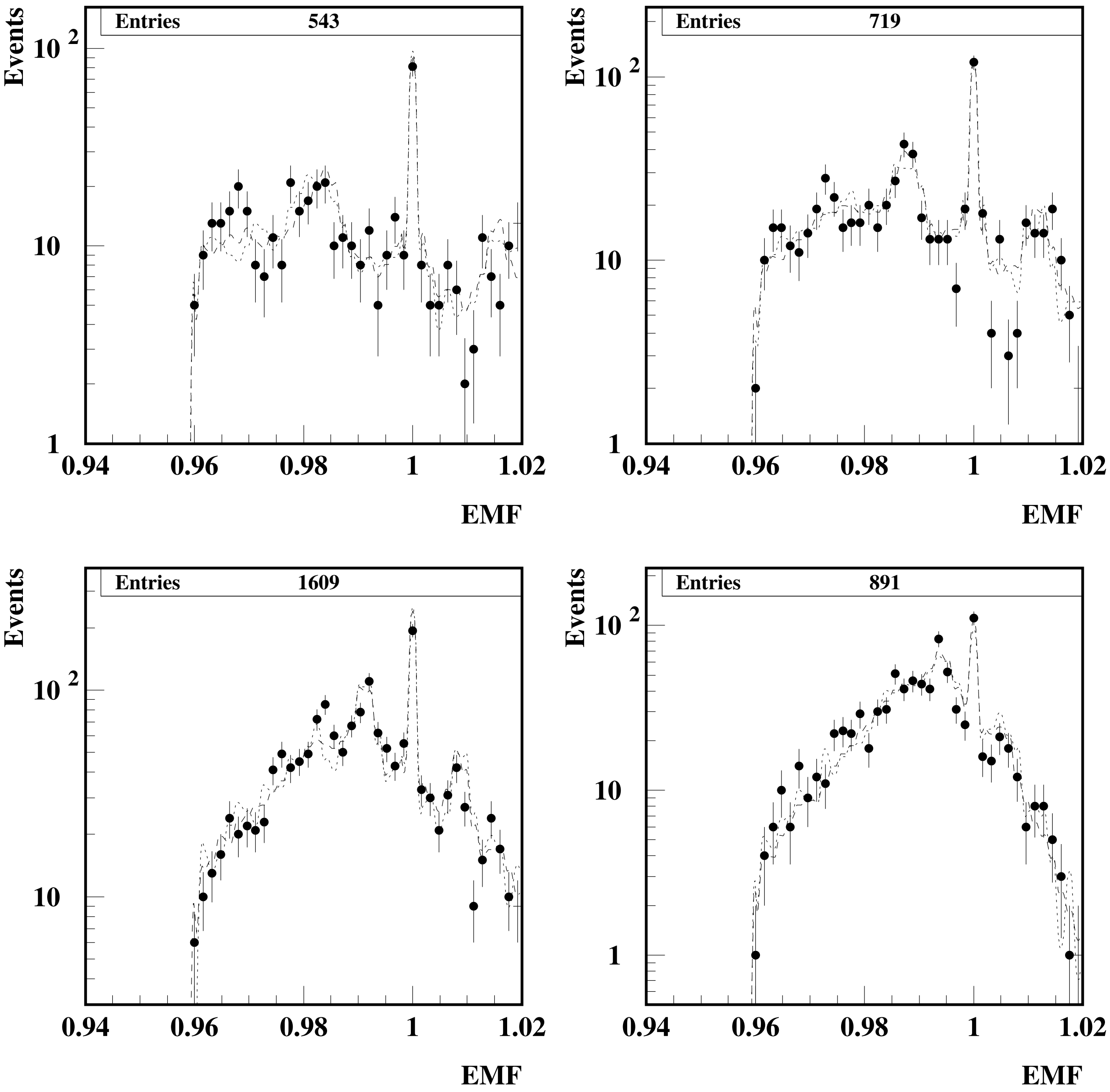

Figure 25: Distributions of EMF for the central region.

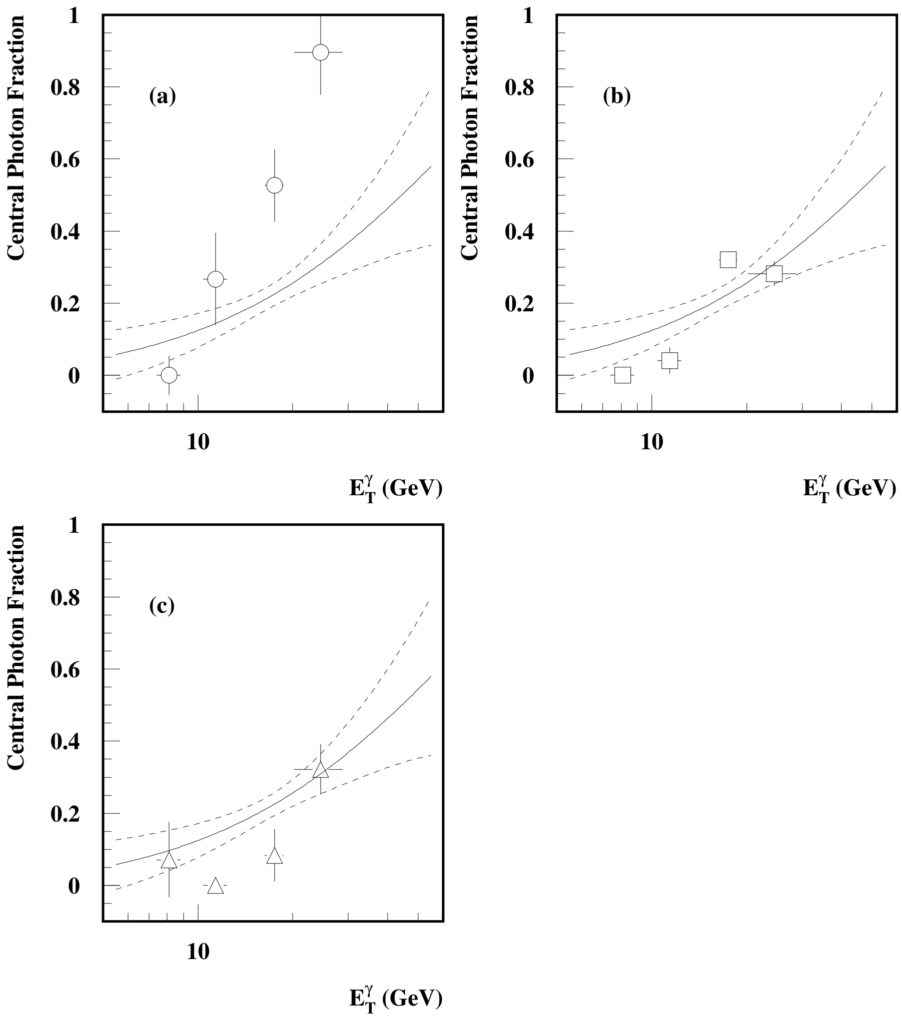

Figure 26: The photon purity in the CC, as extracted from (a) the spread of the em object, (b) the energy deposited in the isolation cones, (c) the result of the χ^2 H-Matrix test. The band correponds to a fit in $\log(E_1/E_{total})$.

References

[1] "The Isolated Photon Cross Section in the Central and Forward Rapidity Region in $p\bar{p}$ Collisions at $\sqrt{s}$=1.8 TeV".
D0 Collab., Phys. Rev. Letters (77), 5011, (1996)

[2] "The Inclusive Cross Section for Isolated Photons in Run 1a",
S.L. Linn, DØ Note ♯ 2745, 1995.

[3] "Inclusive Direct Photon Production in the Central and Forward Rapidity Regions in Proton-Antiproton Collisions at a Center of Mass Energy of 1800 GeV",
S.A. Jerger, Ph.D. Thesis, Michigan State University, 1997.

[4] "The Isolated Photon Cross Section at $\sqrt{s}$ = 1.8 TeV Using the Combined Run 1A/B Data Sample
S.L. Linn,DØ Note ♯ 3564, 1999 .

[5] "The 630 GeV Isolated Direct Photon Cross Section",
S. Grinstein, R. Piegaia, DØ Note ♯ 3350, 1997.

[6] "Producción de Fotones Directos en Colisiones $p\bar{p}$ a 630 GeV",
S. Grinstein, Tesis de Licenciatura, Universidad de Buenos Aires, 1997.

[7] UA2 Collaboration, J. Alitti *et. al.,* Phys. Lett. **B283** (1991) 554.

[8] CDF Collaboration, F. Abe *et. al.,* Phys. Rev. Lett. **73** (1994) 2662; http://www-cdf.fnal.gov/physics/new/qcd/QCD.html.

[9] S.L. Linn, private communication.

[10] A. Schaffer and S.L. Linn, private communication.

[11] D. Owens, Phys. Rev, **D42**, (1990) 61